NUMERICAL TECHNIQUES FOR THE REPRESENTATION OF MOUNTAINS

Fedor Mesinger and Zaviša I. Janjić*
Department of Physics and Meteorology, University of Belgrade

Summary: Problems of the representation of mountains in terrain-following coordinate systems are reviewed, in particular the pressure gradient force error problem. Our ECMWF Seminar 1983 paper on the pressure gradient force and the hydrostatic equation schemes is taken as the starting point. Error calculations are presented for three additional sigma system schemes, and one additional temperature profile. One of these schemes is the Arakawa (1972) scheme, in combination with the Brown-Phillips definition of layer pressures. Another is a scheme obtained by a straightforward correction of the convergence problem of that scheme. The third is a recently proposed "θ-conserving" scheme of Arakawa and Suarez, expanded to include horizontal differencing. Following-up on our Seminar 1983 review of the properties of the alternative step-mountain system, results of subsequent analyses of the properties of the wall boundary condition and the (two-dimensional) scheme for calculation of the potential to kinetic energy conversion are presented. Finally, real data experiments performed to test the performance of the step-mountain system are reviewed. They include cases of Alpine lee cyclogenesis, done both using the step-mountain as well using as the sigma system, and a case of redevelopment apparently triggered by the southern tip of the Appalachian Mountains.

---

* Lecture presented by F. Mesinger

1. INTRODUCTION

Numerical techniques dealing with the representation of mountains in atmospheric models depend on the choice of the vertical coordinate. After being proposed by Phillips (1957), the sigma coordinate has quickly become widely used in atmospheric models (e.g., WMO-ICSU, 1974). In its original form, or modified so as to still keep the main idea of the terrain-following lowest coordinate surface, it perhaps seemed to offer the only way of avoiding uncomfortable problems with the lowest boundary condition.

A problem that has received attention rather early in the development of sigma system models is that of the non-cancellation of errors in the two terms of the pressure gradient force (Smagorinsky et al., 1967). A number of analyses of and many techniques aimed at reducing the error have been put forth; they are summarized at some length in our mentioned review paper (Mesinger and Janjić, 1984). In particular, it has been pointed out that currently used pressure gradient force schemes can be derived as a result of a three-step procedure consisting of (i) calculation of geopotential at terrain following coordinate surfaces, (ii) linear extrapolation/interpolation to constant pressure surfaces, and (iii) evaluation of the pressure gradient force on the constant pressure surfaces. The importance of a "coherency", or "hydrostatic consistency" of the techniques corresponding to steps (i) and (ii) has been stressed by Rousseau and Pham (1971) and Janjić (1977). Otherwise, the slope of the sigma (or other terrain-following coordinate) surface is calculated using one difference formula, and the correction needed to arrive at the slope of the constant pressure surface using another. If the slope of the sigma surface is large, a large error then should come as no surprise.

However, as also pointed out by Janjić, even the hydrostatically consistent

schemes do not guarantee that the error will always be small, since their hydrostatic consistency is lost for steep slopes of sigma surfaces and/or thin sigma layers. As a result, in situations in which substantial errors may be expected (e.g., sharp changes in lapse rate), an increase in vertical resolution, in spite of an associated increased formal accuracy, should be expected to lead to an increase in the error (Mesinger, 1982). Contrary to some published optimistic views (Nakamura, 1978; Sundqvist, 1979), these errors can be large even for carefully designed schemes: say, in terms of geostrophic wind, of the order of 10 m s^{-1} for realistic mountain slopes and grid distances of about 150 km (Mesinger, 1982; Mesinger and Janjić, 1984). While perhaps no direct evidence exists of the detrimental effects of errors of this kind in real data integrations, it appears prudent to avoid even occasional occurrence of such errors, if possible.

From the point of view of this problem with steep slopes and/or thin sigma layers, probably the best sigma system technique is that of explicit vertical interpolation to the desired constant pressure surface, as recently proposed by Mahrer (1984). This, in fact, is the very first method suggested to handle the difficulty (Smagorinsky et al., 1967; Kurihara, 1968, Miyakoda, 1973), which has been used at the Geophysical Fluid Dynamics Laboratory ever since. Recently, the explicit interpolation method has been addressed also by Tomine and Abe (1982), and by Mihailović and Janjić (1986); in the latter paper a scheme conserving energy in conversion between the potential and kinetic energy is presented. In addition to the inherent complexity of calculations, which can make vectorization difficult, the problem of this technique is that it cannot be applied near the ground, where extrapolation to obtain subterranean geopotentials is needed (Mesinger and Janjić, 1984). The possibility of evaluating the pressure gradient force with reduced horizontal grid-step only along the model constant pressure surface which is above the ground hardly

seems attractive in view of the severe linear stability penalty that this might impose (Mahrer, 1984).

A related, still more recent proposal is that of Zheng and Liou (1986). They split the pressure gradient force into its initial value and a departure from the initial value, and calculate only the initial value on pressure surfaces. In this way Zheng and Liou avoid perhaps time-consuming vertical interpolations following the initial time. However, at the initial time the method obviously shares with the straightforward vertical interpolation technique the mentioned problem of extrapolation near the ground. An additional weakness of the method is the lack of an effort to reduce errors in the part of the pressure gradient force which represents the change from the initial state. The method thus, in fact, deals with the analysis and not with the forecasting problem. It is equivalent to the earlier "reference atmosphere" technique of Phillips (1973) and Gary (1973), with the initial state chosen to represent the reference atmosphere.

It is possible that the noise generation due to the sigma system is having a systematic effect on nonlinear interactions and therefore on the spectral distribution of energy, which could be linked to the widespread eddy vs. zonal kinetic energy problem of numerical models (Sadourny, 1985).

With potential temperature used as the vertical coordinate, simulation of the resting atmosphere is possible, since the coordinate surfaces of the resting atmosphere are then horizontal irrespective of the slope of the ground surface. In addition, with the pressure gradient force being a potential vector, its difference formulation can hardly be chosen in a hydrostatically inconsistent way. However, the error problem due to the slope of coordinate surfaces, for an atmosphere in motion, still remains (Mesinger and Janjić, 1984). Thus, with

straightforward schemes, hydrostatic consistency may again be lost for steep slopes of isentropic surfaces and/or thin isentropic layers. For an analysis of various situations as well as possible techniques of maintaining consistency the reader is referred to the Appendix of the recent paper by Mattocks and Bleck (1986). The isentropic coordinate, of course, owes its appeal to features other than the representation of mountains (e.g., Sadourny, 1984).

The use of pressure as the vertical coordinate, or of the geometric height, do not offer advantages comparable to those of isentropic coordinates. The technical difficulties, on the other hand, remain about the same. Thus, one would not expect these choices to gain in popularity. Indeed, a major operational forecasting model that had the pressure vertical coordinate, that of the United Kingdom Meteorological Office, has several years ago been replaced by a model formulated in terms of the sigma coordinate (e.g., Cullen, 1985).

In continuation of this lecture, we shall first return to the analysis of the problems of terrain-following systems. Subsequently, we shall deal with some aspects of the step-mountain system which have not been covered by our 1983 lecture. Finally, we shall present and discuss real data tests of the step-mountain system. They will include two experiments done by performing integrations differing only in the choice of the vertical coordinate, comparing the performance of the step-mountain against that of the sigma system.

2. THE SIGMA SYSTEM PRESSURE GRADIENT FORCE ERRORS

The mentioned results on the possibility of large values of sigma system pressure gradient force errors have been obtained for two schemes using temperature as time dependent variable. Schemes using potential temperature, such as those of Arakawa (1972) and Arakawa and Suarez (1983), or some of their variants, may perhaps be found more appealing on formal or other grounds.

They are apparently used in several major forecasting centers. A report on error calculations done for three schemes of this type should therefore be of interest. At the same time, it will serve as another illustration of the problem at hand.

The Arakawa (1972) vertical differencing scheme has been constructed so as to maintain discrete analogs of four integral constraints satisfied by the continuous equations. These are, as formulated by Arakawa and Suarez (1983), the following.

(I) That the pressure gradient force generates no circulation of vertically integrated momentum along a contour of the surface topography.

(II) That the finite-difference analogues of the energy conversion term have the same form in the kinetic energy and the thermodynamic equations.

(III) That the global mass integral of the potential temperature θ be conserved under adiabatic processes.

(IV) That the global mass integral of a function of θ, such as θ^2, or $\ln\theta$, be conserved under adiabatic processes.

Brown (1974) has extended the Arakawa scheme by deriving an equation layer pressures have to satisfy for the temperatures at these pressures to be equal to the layer pressure-averaged temperatures in case potential temperatures are constant in each layer. Phillips (1974) has shown that errors of temperature when it is calculated using the Arakawa scheme from given values of geopotential can be intolerably large unless an equation of this type is observed. Tokioka (1978) has further analyzed these matters and has shown, inter alia, that use of the Brown equation gives exact values of potential temperature from given values of geopotential when the atmosphere is isentropic.

There are, however, two problems with the Arakawa (1972) scheme. As pointed out by Janjić (1977), it is a hydrostatically inconsistent scheme. It contains one difference analogue of the hydrostatic equation within the geopotential gradient ("first") term of the pressure gradient force, and another in the pressure gradient ("second") term.

The second problem of the scheme is with its hydrostatic equation. Because of the feature of having the geopotential of the lowest layer depend on all the potential temperatures of the vertical column, the scheme, as shown by Arakawa and Suarez (1983), does not represent a convergent analog of the continuous equations.

Nevertheless, the Arakawa (1972) scheme, along with the Brown definition of layer pressures, is used in the U.S. National Meteorological Center's (NMC) spectral model (Sela, 1982). For that reason, as well as for comparison against errors of other schemes, we shall show some results of recent calculations of errors of that scheme (Mesinger, 1987). Previously (Mesinger, 1982; note, however, corrections of some of the Burridge-Haseler scheme values in Mesinger and Janjić, 1984), error calculations have been performed for two schemes, and for two temperature profiles. These were the two profiles (the "no inversion case" and the "inversion case") shown in Fig. 1. As in several earlier calculations, two neighboring surface pressure points were considered located along the direction of the x-axis at pressures of 1000 and 800 mb, respectively. Errors were calculated for a wind point located in between the two surface pressure points, and within the layer centered at $\sigma=0.9$. Calculations were performed for $\Delta\sigma=1/5$, covering the layer extending from 800 to 1000 mb, and for $\Delta\sigma=1/(3\times5)$, $\Delta\sigma=1/(5\times5)$, etc., and in the limit as $\Delta\sigma\rightarrow0$. Pressure gradient force errors have been expressed in fictitious differences in geopotential between the neighboring (temperature) grid

points. In calculating the errors, values of geopotential have been considered exactly known at levels where they are carried by the scheme, simulating in this way an exact analysis of geopotential.

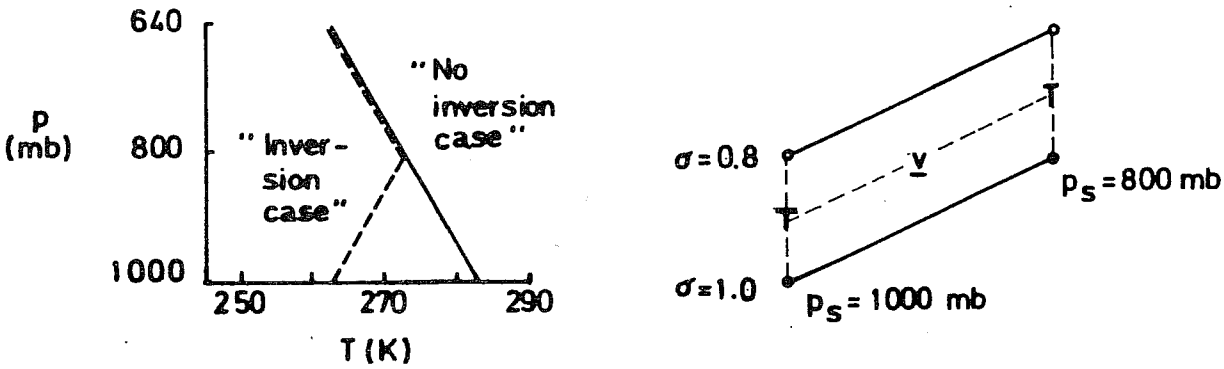

Fig. 1. The temperature profiles and the location of the grid point at which pressure gradient force errors were calculated by Mesinger (1982).

Errors of the Arakawa-Brown scheme have been calculated for the same two temperature profiles, and, in addition, for an isentropic atmosphere. The isentropic atmosphere was defined to have the thermodynamic temperature equal to 273 K at 800 mb, the same as the that of the two profiles shown in Fig. 1. Also the same vertical setup was used, with sigma layers of equal thickness; however, errors have now been calculated for all of the sigma layers. Thus, errors have been calculated for 5, 15, 25, ... sigma layers from the top (p=0) to the ground surface of the model atmosphere.

Rather large errors have been obtained for the inversion and also for the no inversion case: of the order of 20-30 m in height differences between the neighboring temperature points. Values over 40 m were not uncommon, and at one point even a value of over 80 m was obtained (the inversion case, 5 layers). For illustration, results for 25 layers, and for the three profiles, are shown in Fig. 2. Not surprisingly, little tendency, if any, could be noticed for errors to

decrease with increasing resolution. For example, errors of 45 layer resolution were for both the no inversion as well as for the inversion case clearly greater than those shown in the figure.

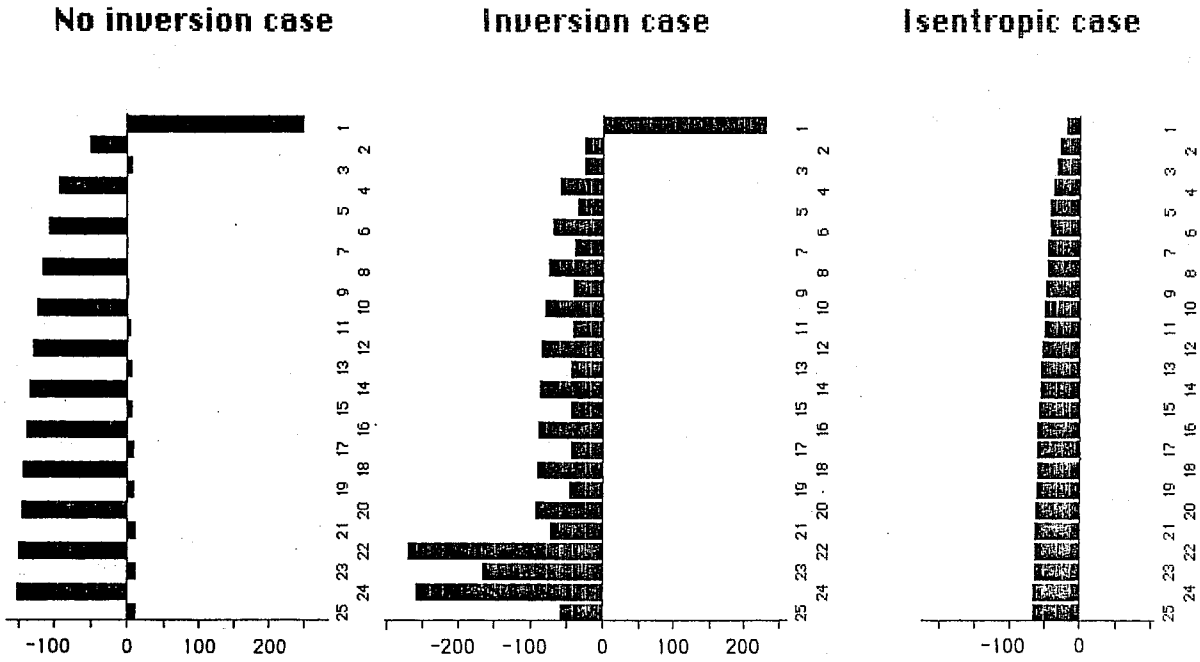

Fig. 2. Errors of the Arakawa (1972) - Brown (1974) pressure gradient force scheme, for the "no inversion case" (left hand panel), "inversion case" (middle panel) and an isentropic atmosphere (right hand panel), for a vertical structure of 25 sigma layers of equal thickness. Values are given in increments of geopotential ($m^2 s^{-2}$), between two neighboring grid points, along the direction of the increasing terrain elevations.

The obtained errors are generally much greater than those reported earlier for the Corby et al. (1972) and for the Burridge and Haseler (1977) schemes. One might suspect that these rather large values at the relatively high vertical resolutions considered are primarily a result of the feature of the scheme of not representing a convergent analog of the continuous pressure gradient force expression. Therefore, a comparison against errors of a scheme in which this feature is removed may be of interest. Such is the scheme used in the NMC "Nested Grid Model" (NGM; Hoke et al., 1985), and apparently also in the Japan Meteorological Agency hemispheric spectral model (JMA, 1986, p. 23). In this scheme, which we shall call the NGM scheme, the Arakawa (1972) equation for

the lowest layer geopotential has been replaced by a simple uncentered scheme resulting from an assumption that the potential temperature is constant from the surface to the lowest temperature ("full") level, and equal to the potential temperature of that layer.

Errors obtained for the NGM scheme, for the same two profiles and resolutions, have indeed been generally smaller than those of the original Arakawa-Brown scheme. This may not be not quite so evident from the 25 layer values which are shown in Fig. 3. This is due to the Arakawa-Brown 25 layer errors, shown in Fig. 2, fortuitously being smaller than have generally been the errors of the scheme for both the lower as well as the higher vertical resolutions. In Fig. 3 the isentropic atmosphere values are not shown, since in case of the isentropic atmosphere there is no difference between the two schemes. What is evident from Fig. 3 is that the amplitude of the NGM scheme errors for the two profiles

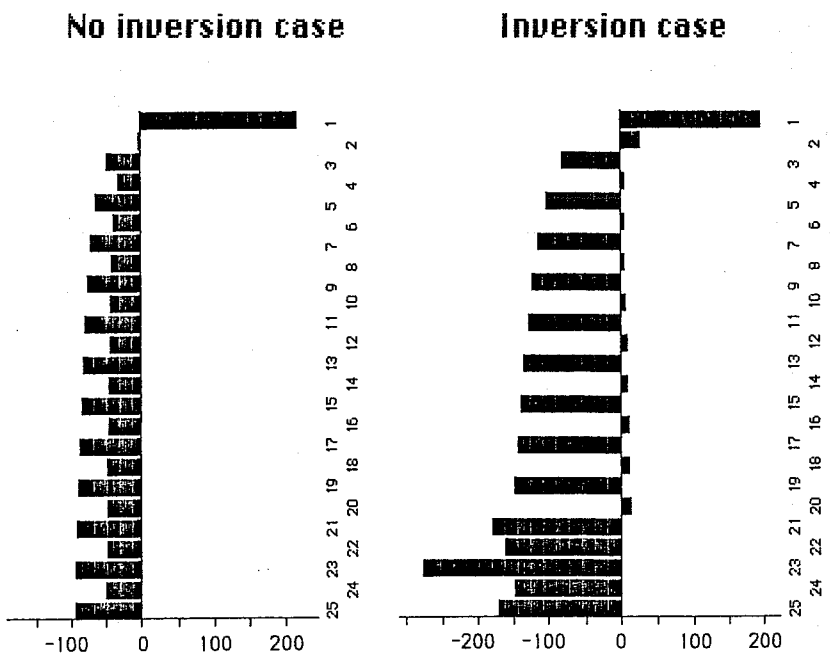

Fig. 3. Errors of the Nested Grid Model (see text for details) pressure gradient force scheme, for the "no inversion case" (left hand panel), and the "inversion case" (right hand panel), for a vertical structure of 25 sigma layers of equal thickness. Values are given in increments of geopotential ($m^2 s^{-2}$), between two neighboring grid points, along the direction of the increasing terrain elevations.

considered is, just as that of the original Arakawa-Brown scheme errors, very much dominated by a false vertical two grid interval wave. Apparently neither the Brown equation for layer pressures nor the removal of the convergence problem are fully effective in eliminating the fictitious vertical oscillation problem of the scheme-pointed out by Phillips (1974).

The remaining vertical differencing problem of the scheme, that of the hydrostatic inconsistency, can of course also be removed. Indeed, the Arakawa and Suarez (1983) "local" hydrostatic equation and pressure gradient force schemes are free of the hydrostatic consistency problem. Within the family of schemes they have considered, of most interest perhaps is the so-called θ-conserving scheme. This is a scheme which, while abandoning just as the NGM scheme the feature (IV) of the Arakawa (1972) scheme of the conservation of the integral of a function of θ, in return achieves a number of other appealing properties (Arakawa and Suarez, 1983, p. 44). It is used at the U.S. Naval Environmental Prediction Research Facility (Rosmond, personal communication), as well as the NASA/Goddard Space Flight Center Laboratory for Atmosphere (Kalnay, personal communication).

Following the setup used for the preceding two schemes, Mesinger has calculated the errors also for the Arakawa-Suarez θ-conserving scheme. For error calculations, the scheme had to be expanded to include horizontal differencing; a momentum conserving horizontal differencing was used (along the lines of, for example, Eq. (291) of Arakawa and Lamb, 1977).

Reduction of errors due to to the removal of the hydrostatic inconsistency in vertical differencing, if any, was not impressive. For comparison against errors of the two preceding schemes, the 25 layer values are shown in Fig. 4. Once more, the isentropic atmosphere values are not shown, since in case of the

the isentropic atmosphere the scheme again reduces to the Arakawa-Brown scheme. As with the two preceding schemes, there was little evidence of the errors being reduced with an increase in vertical resolution.

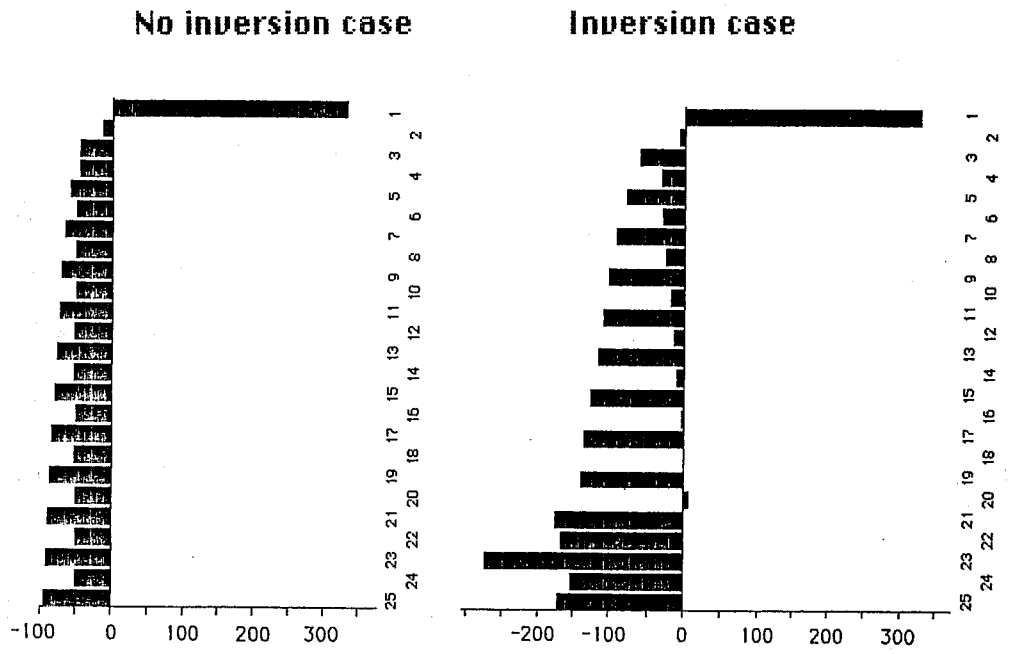

Fig. 4. Errors of the Arakawa-Suarez θ-conserving pressure gradient force scheme, expanded to include horizontal differencing, for the "no inversion case" (left hand panel), and the "inversion case" (right hand panel), for a vertical structure of 25 sigma layers of equal thickness. Values are given in increments of geopotential ($m^2 s^{-2}$), between two neighboring grid points, along the direction of the increasing terrain elevations.

A puzzling feature of these calculations is the very large error at the top layer. The top layer error was found to increase with increasing resolution; for example, the top layer errors of the 45 layer Arakawa-Suarez calculations amounted to about 500 $m^2 s^{-2}$ for both the no inversion as well as for the inversion case.

Errors of the Arakawa-Suarez scheme of the magnitude of the errors displayed in Fig. 4 may perhaps be found surprising in view of the scheme not suffering from either of the two mentioned undesirable features of the vertical

differencing of the Arakawa-Brown scheme. Possibly these large values are a result of the scheme being optimized for the isentropic atmosphere case, a profile rather different from the two profiles which in calculations reported on here have resulted in large errors.

In comparison with the situation as reviewed in our 1983 lecture, the results for schemes carrying potential temperature as time dependent variable summarized in this section offer little additional encouragement for the use of conventional sigma system schemes above steep mountains. They do seem to encourage further studies of the problem, including exploration of alternative approaches.

3. OTHER SIGMA SYSTEM PROBLEMS

Several other problems are associated with terrain following coordinates. Dynamical processes may be distorted by the irregularities inherent to a sigma-type grid (Sadourny et al., 1981). Technical problems are that of the need for vertical interpolations of pressure surface data or analyses, and that of the lateral/horizontal diffusion (e.g., Simmons and Burridge, 1981).

Experiments using the ECMWF model have revealed a tendency for excessive precipitation to occur over some mountainous areas, as a result of diffusion calculated on sigma surfaces. A reduction of the excessive rainfall was achieved by applying the horizontal diffusion not to the temperature alone, but to the temperature modified by the addition of a correction term approximating the diffusion of temperature on pressure surfaces (Simmons and Jarraud, 1984). However, beneficial effects of some of the excessive rainfall in terms of an improved simulation of the tropical general circulation have been noted by Tibaldi (1986).

Sensitivity of unexpected amplitude to the formulation of lateral diffusion on pressure vs. on sigma surfaces has recently been noted by Michaud and Sadourny (1986). Compared to the control sample of five January sigma diffusion simulations, in another ensemble of four pressure diffusion simulations many large-scale structures have been better simulated in both midlatitudes and tropics; variability has been equally improved.

4. THE STEP-MOUNTAIN SYSTEM

Definition. One of the alternative approaches is the step-mountain system, representing, in fact, a simple modification of the sigma system. The vertical coordinate of the system, Mesinger (1984), can be written as

$$\eta = \frac{p - p_T}{p_S - p_T}\,\eta_S \qquad (1)$$

with

$$\eta_S = \frac{p_{rf}(z_S) - p_T}{p_{rf}(0) - p_T}\,. \qquad (2)$$

Here p is pressure, the subscripts T and S stand for the top and the ground surface values of the model atmosphere, respectively; z is geometric height, and $p_{rf}(z)$ is a suitably defined reference pressure as a function of z. Furthermore, the ground surface heights z_S are permitted to take only a discrete set of values, chosen so that mountains are constructed from the three-dimensional grid boxes in the model. If this is felt to be advantageous, say to reduce the occurrence of steps within the planetary boundary layer, $p_{rf}(0)$ in (2) can be replaced by $p_{rf}(z_b)$, with z_b representing a base elevation defined so as to include gentle slopes of the surface topography. For example, elevations less than a given value could be represented by z_b, while those higher could be represented by steps.

A schematic picture of the representation of mountains using this

"step-mountain" coordinate is shown in Fig. 5. In this figure, u, T, and p_s represent the u velocity component, temperature, and surface pressure grid points, respectively. The circled u grid points are the points with zero values of the velocity components normal to sides of the mountain shown in the figure.

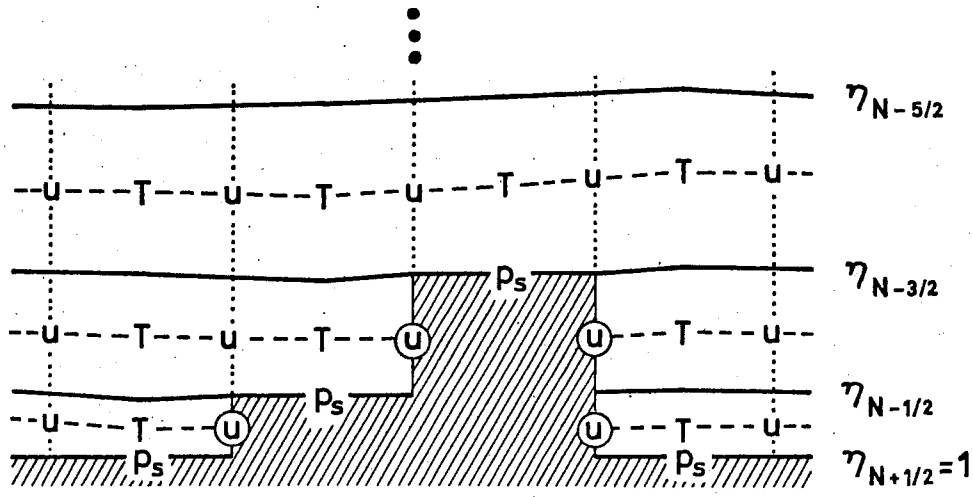

Fig. 5. A schematic picture of the representation of mountains using the coordinate (1)-(2).

An attractive feature of (1) is that, once a model code using (1) has been written, an option of having at all grid points $\eta_s = 1$ can easily be included. Thus, the same code can be run as a step-mountain (referred to as "eta") and as a sigma system model. This, obviously, enables a comparison of the performance of the two systems, without the ever present danger of having differences in results produced by a code error. Two experiments of this kind have been performed and will be discussed in the following section.

In our 1983 lecture, generalization of schemes maintaining conservation of momentum and energy, so as to cover the possibility of the step-mountain coordinate, has been presented. However, considerations have been restricted to the one-dimensional case. Extension to two horizontal dimensions, for horizontal grid and schemes that have been used for mentioned experiments, will be done in the continuation of this section.

Internal boundaries. The step-like mountains introduce the problem of internal boundaries between the free atmosphere and the mountain blocks. This problem is related only to horizontal differencing. Therefore, it is sufficient to consider a barotropic fluid. In addition, for simplicity it is convenient to use the plane geometry.

As the first step, the horizontal grid and locations of the mountain blocks should be specified. We have chosen the Arakawa E grid, with mountain blocks as in Fig. 5 located at height points. On the Arakawa E grid displayed in Fig. 6, an example of grid boxes filled with mountains is shown, with the mountains indicated by shading. As usual, the symbol h in the figure denotes the height of the free surface, **v** is the velocity vector, and d is the distance between the two nearest grid points carrying the same variable. In the mountain discretization procedure, as a simple way of avoiding the creation of temperature points with no neighboring velocity points, groups of four neighboring points were defined to have the same elevation. Thus, the mountain shown in the figure is our "minimum" model mountain. It should be noted, however, that this choice has been made for reasons other than the internal boundary scheme formulation, and that the analysis of this subsection will in fact be applicable to mountains formed of an arbitrary number of neighboring height points, including single ones.

At the velocity points located along the internal boundaries we choose the no-slip boundary condition, i.e.,

$$\mathbf{v}=0. \tag{3}$$

In this subsection, following Janjić and Ničković (Mesinger et al., 1987), properties will first be examined of horizontal advection schemes obtained when fictitious velocity points are introduced inside the mountains at places where velocity points would be located were the mountains absent. At these

points, Janjić and Ničković assume that

$$\Psi_{ground}=0. \qquad (4)$$

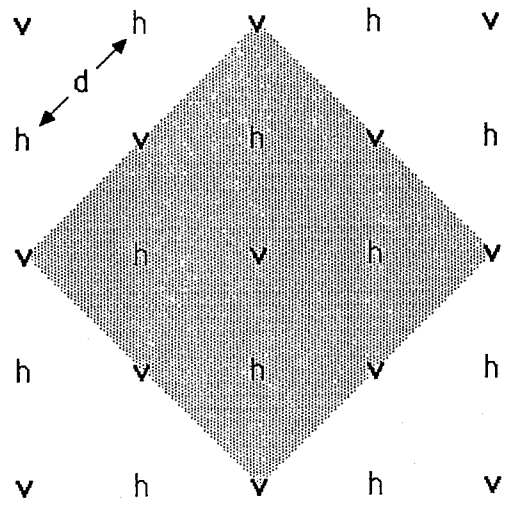

Fig. 6. Grid E with "minimum-extension" four-point step-mountain indicated by shading.

In order to check whether, and if so to what extent, the internal boundaries affect the conservation properties of the advection schemes used in the model, it is convenient to start with a review of several properties of the E grid. Following Janjić (1984), the velocity field on the E grid can be represented in terms of the stream function ψ and velocity potential χ, as shown in Fig. 7. Note, furthermore, that an Arakawa staggered C grid can be introduced with the ψ points coinciding with those of the E grid; this in fact has been done to arrive at the advection scheme which will be considered here. Two coordinate systems, x,y and x',y', rotated by 45^0 with respect to each other, are also introduced in the figure. The rotational velocity components on the semi-staggered grid E, and on the staggered grid C, can be defined applying the operator

$$\delta_s\psi=[\psi(s+\Delta s/2)-\psi(s-\Delta s/2)]/\Delta s, \qquad (5)$$

along the coordinate axes x,y and x',y'. The increment Δs in (5) takes on the value $\sqrt{2}d$, or d, depending on whether the operator is applied along the coordinate axes x,y, or x',y'.

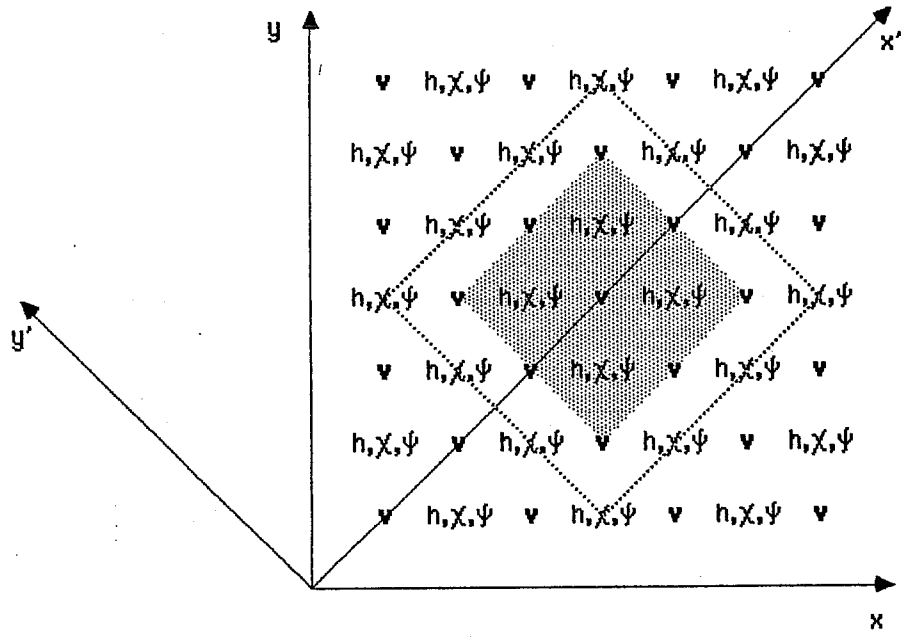

Fig. 7. Grid E with stream function and velocity potential grid points used to define the velocity components along the coordinate axes x,y and x',y'. The mountain blocks are indicated by shading. The constant stream function area is bounded by the dotted line.

It should be noted that in the case of nondivergent flow, (3) and (4) will be satisfied if the stream function is constant at the fictitious points inside the mountain, and at the row of ψ points in the free atmosphere next to the mountain. Janjić and Ničković have assumed this to be the case. The area of constant stream function is indicated in Fig. 7 by the dotted line.

As can be seen from Fig. 7, rotational velocity components in the sense of the C grid are located midway between the nearest ψ points and have the form

$$u_r' = -\delta_{y'}\psi \ , \quad v_r' = \delta_{x'}\psi \ .$$

On the E grid the rotational velocity components are defined by

$$u_r=-\delta_y\psi\ ,\quad v_r=\delta_x\psi\ .$$

Note that within the constant ψ area the rotational velocity components as well as the C and E grid finite-difference analogs of vorticity are equal to zero.

The conservation properties of the horizontal finite-difference schemes are achieved through mutual cancellation of the fluxes between the neighboring points. With the step-mountain approach, this cancellation cannot be accomplished in the entire integration domain because some of the grid points do not have all of the neighboring points required for the cancellations. In this situation, conservation will nevertheless be achieved if the uncompensated fluxes are equal to zero. This will be the case if either of the following two conditions is satisfied:

(i) The velocity component entering the flux definition is equal to zero; or

(ii) The quadratic quantity appearing in the flux definition is defined as a product of the values at two neighboring grid points, and vanishes because the value at the fictitious grid point inside the mountain, or at the points along the side of the mountain, is equal to zero.

The Janjić (1984) E grid horizontal advection scheme conserves the mean enstrophy, vorticity and rotational energy as defined on the staggered grid C. In the case of nondivergent flow, using the E grid rotational velocity components u_r and v_r for the definition of the fluxes, these quantities are governed by the equations

$$\partial(\zeta'^2/2)/\partial t=-(1/3)\{\delta_x[u_r\overline{\overline{\zeta'^2}^y}^x/2]+\delta_y[v_r\overline{\overline{\zeta'^2}^x}^y/2]\}$$
$$-(2/3)\{\delta_{x'}[(\sqrt{2}/2)(\overline{u_r+v_r})^{y'}\overline{\overline{\zeta'^2}^y}^{x'}/2]+\delta_{y'}[(\sqrt{2}/2)(\overline{-u_r+v_r})^{x'}\overline{\overline{\zeta'^2}^x}^{y'}/2]\}\ ,$$

$$\partial\zeta'/\partial t=-(1/3)\{\delta_x[u_r\overline{\zeta'}^x]+\delta_y[v_r\overline{\zeta'}^y]\}$$
$$-(2/3)\{\delta_{x'}[(\sqrt{2}/2)(\overline{u_r+v_r})^{y'}\overline{\zeta'}^{x'}]+\delta_{y'}[(\sqrt{2}/2)(\overline{-u_r+v_r})^{x'}\overline{\zeta'}^{y'}]\}\ ,$$

$$\partial(u_r'^2/2)/\partial t=-(1/3)\{\delta_x[\overline{u_r}^{y'}\overline{u_r'u_r'}^{x}/2]+\delta_y[\overline{v_r}^{y'}\overline{u_r'u_r'}^{y}/2]$$

$$-(2/3)\{\delta_x[(\sqrt{2}/2)\overline{(u_r+v_r)}^{y'}\ \overline{u_r'u_r'}^{x'}/2]+\delta_y[(\sqrt{2}/2)\overline{(-u_r+v_r)}^{x'}\ \overline{u_r'u_r'}^{y'}/2]\}+\dots\ ,$$

$$\partial(v_r'^2/2)/\partial t=-(1/3)\{\delta_x[\overline{u_r}^{x'}\overline{v_r'v_r'}^{x}/2]+\delta_y[\overline{v_r}^{x'}\overline{v_r'v_r'}^{y}/2]$$

$$-(2/3)\{\delta_x[(\sqrt{2}/2)\overline{(u_r+v_r)}^{y'}\ \overline{v_r'v_r'}^{x'}/2]+\delta_y[(\sqrt{2}/2)\overline{(-u_r+v_r)}^{x'}\ \overline{v_r'v_r'}^{y'}/2]\}+\dots\ .$$

Here, ζ' is the vorticity as defined on the C grid, and the expressions of the form $\overline{AA}^{s}$ represent the products of the values of A at two neighboring grid points along the axis s.

Direct inspection of the above equations reveals that at the internal boundaries, the C grid enstrophy is conserved because both conditions (i) and (ii) are satisfied; voriticity and therefore C grid rotational momentum is conserved because condition (i) is satisfied; and, finally, the C grid rotational energy is conserved because condition (ii) is satisfied.

If the divergent part of the flow is included, the continuity equation, the equations governing the evolution of the kinetic energy as defined on the E grid under the advective processes, and the E grid momentum equations have the form (Janjić, 1984)

$$\partial h/\partial t=-\{(1/3)(\delta_x U+\delta_y V)+(2/3)(\delta_{x'}U'+\delta_{y'}V')\}\ ,$$

$$\partial(\overline{h}^{x}u^2/2)/\partial t=-\{(1/3)[\delta_x(\overline{U}^{x}\overline{uu}^{x}/2)+\delta_y(\overline{V}^{x}\overline{uu}^{y}/2)]$$
$$+(2/3)[\delta_{x'}(\overline{U'}^{x}\overline{uu}^{x'}/2)+\delta_{y'}(\overline{V'}^{x}\overline{uu}^{y'}/2)]\}+\dots\ ,$$

$$\partial(\overline{h}^{y}v^2/2)/\partial t=-\{(1/3)[\delta_x(\overline{U}^{y}\overline{vv}^{x}/2)+\delta_y(\overline{V}^{y}\overline{vv}^{y}/2)]$$
$$+(2/3)[\delta_{x'}(\overline{U'}^{y}\overline{vv}^{x'}/2)+\delta_{y'}(\overline{V'}^{y}\overline{vv}^{y'}/2)]\}+\dots\ ,$$

$$\partial(\overline{h}^{x}u)/\partial t=-\{(1/3)[\delta_x(\overline{U}^{x}\overline{u}^{x})+\delta_y(\overline{V}^{x}\overline{u}^{y})]+(2/3)[\delta_{x'}(\overline{U'}^{x}\overline{u}^{x'})+\delta_{y'}(\overline{V'}^{x}\overline{u}^{y'})]\}+\dots ,$$

$$\partial(\overline{h}^{y}v)/\partial t=-\{(1/3)[\delta_x(\overline{U}^{y}\overline{v}^{x})+\delta_y(\overline{V}^{y}\overline{v}^{y})]+(2/3)[\delta_{x'}(\overline{U'}^{y}\overline{v}^{x'})+\delta_{y'}(\overline{V'}^{y}\overline{v}^{y'})]\}+\dots .$$

Here,

$$U=\overline{h}^{x}u , \quad V=\overline{h}^{y}v , \quad U'=\overline{h}^{x'}(\sqrt{2}/2)(\overline{u+v})^{y'} , \quad V'=\overline{h}^{y'}(\sqrt{2}/2)(\overline{-u+v})^{x'} .$$

Again, direct inspection reveals that the mass is conserved because the condition (i) is satisfied, and the E grid kinetic energy is conserved because the condition (ii) is satisfied. However, the E grid momentum is not conserved. Janjić and Ničković decided not to look for another definition of boundary conditions and therefore did not try to enforce the momentum conservation. Possible detrimental effects, if any, were not noticed in the experimental integrations performed so far.

An important process which cannot be treated within the frame of the barotropic model is the temperature advection. However, all relevant information can be obtained by examining the properties of the scheme for the advection of a passive quantity T. The scheme for temperature advection which we use, combined with the continuity equation, takes the form

$$\partial(hT)/\partial t=-\{(1/3)[\delta_x(U\overline{T}^{x})+\delta_y(U\overline{T}^{y})]+(2/3)[\delta_{x'}(U'\overline{T}^{x'})+\delta_{y'}(V'\overline{T}^{y'})]\} .$$

Direct inspection reveals that the condition (i) is satisfied and therefore the first moment of the distribution of T is conserved. Multiplying this equation by T, and taking into account the continuity equation, one easily finds that the second moment is also conserved, again because the condition (i) is satisfied.

Thus, with the internal boundary conditions specified as above, except for the E grid momentum, all favorable conservation properties of the Janjić (1984) E grid advection schemes are preserved.

Another internal boundary problem we have looked into is that of the mass conservation within the modification of the continuity equation designed to supress the E (or B) grid two-grid-interval noise (Mesinger, 1973; Janjić, 1979). As this modification, the term proportional to

$$-(\nabla_{\times}\cdot\mathbf{P}' - \nabla_{+}\cdot\mathbf{P}) \tag{6}$$

is added to the right hand side of the surface pressure tendency equation. Here $\nabla_{\times}\cdot$ and $\nabla_{+}\cdot$ are the divergence operator analogs, and $\mathbf{P}'$ and $\mathbf{P}$ pressure gradient force analogs, calculated along the axes x',y' and x,y, respectively (Janjić, 1979; see also Cullen, 1983).

In the model used for the experiments, however, (6) is replaced by

$$-\frac{1}{2}(\overline{\Pi}^{x} - \overline{\Pi}^{y}), \tag{7}$$

where

$$\Pi \equiv \delta_{x'}P_{y'} + \delta_{y'}P_{x'}.$$

Note that with pressure gradient force a potential vector, as for example in the simple shallow water case, there is no difference between the analogs (6) and (7).

A term proportional to (7) at a height point consists of contributions proportional to values of Π at four neighboring velocity points. With no internal boundaries, and inside the integration region, these contributions from velocity points are added to values of surface pressure at two of the four surrounding height points. At the remaining two of the surrounding height points they are subtracted from the values of surface pressure. Thus, no false change of mass will occur due to the addition of a term proportional to (7) to the surface pressure tendency equation.

To maintain mass conservation with internal boundaries present, we have set values of Π equal to zero at all velocity points located at the sides of

mountains. A similar procedure is used to maintain mass conservation at the lateral boundaries of the integration region. To this end, values of Π are set to zero along the first (outermost) row of velocity points of the integration domain of the model. This is the first row of points following the two rows of points which are used for specification of the lateral boundary conditions of the model.

Energy conservation and the $\omega\alpha$ term. In this subsection, following Gavrilov (Mesinger et al., 1987), the procedure will be outlined leading to an energy conserving scheme for the $\omega\alpha$ term of the η coordinate thermodynamic equation. As we shall see, this procedure is analogous to that used in the σ coordinate system.

The zonal and meridional components of the pressure gradient force, denoted respectively by PGFU and PGFV, are defined at the **v** points, and at model's layer k have the form

$$PGFU_k = -1/(2h_1\Delta\lambda)\{(1/3)[(\Delta_\lambda \overline{\Phi^{\eta}}^{\lambda'\psi'} + \Delta_{-\psi}\overline{\Phi^{\eta}}^{\lambda'\psi'})$$

$$+(RT/\overline{p^{\eta}}^{\lambda'\psi'})\Delta_\lambda \overline{p^{\eta}}^{\lambda'\psi'} + (RT/\overline{p^{\eta}}^{\lambda'\psi'})\Delta_{-\psi}\overline{p^{\eta}}^{\lambda'\psi'}]$$

$$+(2/3)(1/\Delta\overline{p}^{\lambda})[(\Delta\overline{p}^{\lambda'\psi'}\Delta_\lambda \overline{\Phi^{\eta}}^{\lambda'\psi'} + \Delta\overline{p}^{\lambda'\psi'}\Delta_{-\psi}\overline{\Phi^{\eta}}^{\lambda'\psi'})$$

$$+\Delta\overline{p}^{\lambda'\psi'}(RT/\overline{p^{\eta}}^{\lambda'\psi'})\Delta_\lambda \overline{p^{\eta}}^{\lambda'\psi'} + \Delta\overline{p}^{\lambda'\psi'}(RT/\overline{p^{\eta}}^{\lambda'\psi'})\Delta_{-\psi}\overline{p^{\eta}}^{\lambda'\psi'}]\}_k ,$$

$$PGFV_k = -1/(2h_2\Delta\psi)\{(1/3)[(\Delta_{\lambda'}\overline{\Phi}^{\eta}{}^{\psi'}{}^{\lambda'} - \Delta_{-\psi'}\overline{\Phi}^{\eta}{}^{\psi'}{}^{\lambda'})$$

$$+(RT/\overline{p}^{\eta})\Delta_{\lambda'}\overline{p}^{\eta}{}^{\psi'}{}^{\lambda'} - (RT/\overline{p}^{\eta})\Delta_{-\psi'}\overline{p}^{\eta}{}^{\psi'}{}^{\lambda'}]$$

$$+(2/3)(1/\Delta\overline{p}^{\psi})[(\Delta\overline{p}^{\lambda'}\Delta_{\lambda'}\overline{\Phi}^{\eta}{}^{\psi'}{}^{\lambda'} - \Delta\overline{p}^{\psi'}\Delta_{-\psi'}\overline{\Phi}^{\eta}{}^{\psi'}{}^{\lambda'})$$

$$+\Delta\overline{p}^{\lambda'}(RT/\overline{p}^{\eta})\Delta_{\lambda'}\overline{p}^{\eta}{}^{\psi'}{}^{\lambda'} - \Delta\overline{p}^{\psi'}(RT/\overline{p}^{\eta})\Delta_{-\psi'}\overline{p}^{\eta}{}^{\psi'}{}^{\lambda'}]\}_k .$$

Here, h_1 and h_2 are the metric coefficients defined by

$$h_1 = 1/(a\cos\psi), \quad h_2 = 1/a ,$$

where a is the radius of the Earth, and λ and ψ are longitude and latitude respectively. The distances between two neighboring mass and wind points in the directions of the coordinate axes λ and ψ are denoted by $\Delta\lambda$ and $\Delta\psi$, respectively. The depths of the η layers in terms of pressure are denoted by Δp. The axes λ' and ψ' are defined by analogy with the "diagonal" coordinate axes x' and y' used in the plane geometry in the subsection dealing with the internal boundaries. The symbol Δ represents centered differences calculated along the axes indicated by the subscripts. The subscripts with negative signs indicate that the differences are calculated in the negative directions of the axes. Unless otherwise stated, as before, the overbars denote the simplest two-point averaging in the direction of the coordinate axis indicated by the accompanying superscript. The other symbols used have their usual meaning.

Dealing with the kinetic energy generation, it is convenient to split both the

"1/3" and "2/3" terms into their geopotential and pressure gradient parts, and then to consider separtely the contribution of each of the four terms obtained in this way. Summing up the contributions of the geopotential gradient part of the "1/3" term over the **v** points, excluding the points inside the mountains, one obtains

$$E_1=\Sigma_{\mathbf{v}} -(1/3)\,(\Delta A/g)\,\{\, u\Delta\overline{p}^{\lambda}/(2h_1\Delta\lambda)\,[\,\Delta_{\lambda'}\overline{\Phi}^{\eta}+\Delta_{-\varphi'}\overline{\Phi}^{\eta}\,] + v\Delta\overline{p}^{\varphi}/(2h_2\Delta\varphi)\,[\,\Delta_{\lambda'}\overline{\Phi}^{\eta}-\Delta_{-\varphi'}\overline{\Phi}^{\eta}\,]\,\}_k\,, \tag{8}$$

where $\Delta A=4h_1h_2\Delta\lambda\Delta\varphi$ and g is gravity. As (8) is to be used to determine an analog to $\kappa T\omega/p$ ($\omega\alpha$ term) carried at T points, the summation over the **v** points should be replaced by the summation over the T points in the free atmosphere. Assuming the cyclic boundary conditions, or a closed integration domain, after some algebra, (8) can be rewritten in the form

$$E_1=\Sigma_T\,(1/3)\,(\Delta A/g)\,\overline{\Phi_k}^{\eta}\,/\,(2h_1h_2\Delta\lambda\Delta\varphi)\,[\Delta_{\lambda}(u\Delta\overline{p}^{\lambda}h_2\Delta\varphi)+\Delta_{\varphi}(v\Delta\overline{p}^{\varphi}h_1\Delta\lambda)]_k\,. \tag{9}$$

Here, the fluxes across the internal boundaries are set to zero in accordance with the boundary condition (3).

In a similar way, the pressure gradient part of the "1/3" term yields

$$E_2=\Sigma_{\mathbf{v}} -(1/3)\,(\Delta A/g)\,\{\, u\Delta\overline{p}^{\lambda}/(2h_1\Delta\lambda)\,[\,(RT/\overline{p}^{\eta})\Delta_{\lambda'}\overline{p}^{\eta}+(RT/\overline{p}^{\eta})\Delta_{-\varphi'}\overline{p}^{\eta}\,] + v\Delta\overline{p}^{\varphi}/(2h_2\Delta\varphi)\,[\,(RT/\overline{p}^{\eta})\Delta_{\lambda'}\overline{p}^{\eta}-(RT/\overline{p}^{\eta})\Delta_{-\varphi'}\overline{p}^{\eta}\,]\,\}_k\,,$$

and, after rearrangement,

$$E_2=\Sigma_T -(1/3)\,(\Delta A/g)/(2h_1h_2\Delta\lambda\Delta\varphi)$$

$$\{\, uh_2\Delta\varphi\Delta\overline{p}^{\lambda}[(RT/\overline{p}^{\eta})\Delta_{\lambda'}\overline{p}^{\eta} + (RT/\overline{p}^{\eta})\Delta_{-\varphi'}\overline{p}^{\eta}\,] \qquad (10)$$

$$+\, vh_1\Delta\lambda\Delta\overline{p}^{\varphi}[(RT/\overline{p}^{\eta})\Delta_{\lambda'}\overline{p}^{\eta} - (RT/\overline{p}^{\eta})\Delta_{-\varphi'}\overline{p}^{\eta}\,]\,\}_k\,.$$

The kinetic energy generation by the geopotential gradient part of the "2/3" term is given by

$$E_3=\Sigma_{\mathbf{v}} -(2/3)\,(\Delta A/g)\,[u/(2h_1\Delta\lambda)\,(\Delta\overline{p}^{\lambda'}\Delta_{\lambda'}\overline{\Phi}^{\eta} + \Delta\overline{p}^{\varphi'}\Delta_{-\varphi'}\overline{\Phi}^{\eta}) + v/(2h_2\Delta\varphi)\,(\Delta\overline{p}^{\lambda'}\Delta_{\lambda'}\overline{\Phi}^{\eta} - \Delta\overline{p}^{\varphi'}\Delta_{-\varphi'}\overline{\Phi}^{\eta})\,]_k\,,$$

or, after rearrangement,

$$E_3=\Sigma -(2/3)\,(\Delta A/g)/(2h_1h_2\Delta\lambda\Delta\varphi) \qquad (11)$$

$$[\Delta\overline{p}^{\lambda'}(\overline{uh_2\Delta\varphi+vh_1\Delta\lambda}^{\varphi'})\Delta_{\lambda'}\overline{\Phi}^{\eta}+\Delta\overline{p}^{\varphi'}(\overline{vh_1\Delta\lambda-uh_2\Delta\varphi}^{\lambda'})\Delta_{\varphi'}\overline{\Phi}^{\eta}\,]_k\,.$$

Note that this time the summation is not performed over the T points; instead, the expressions under the summation sign are defined in between each pair of nearest T points. However, introducing the notation

$$u'd=\overline{uh_2\Delta\varphi+vh_1\Delta\lambda}^{\varphi'}\,,\quad v'd=\overline{vh_1\Delta\lambda-uh_2\Delta\varphi}^{\lambda'}\,,$$

after some algebra, from (11) one obtains

$$E_3=\Sigma_T -(2/3)\,(\Delta A/g)/(2h_1h_2\Delta\lambda\Delta\varphi)$$

$$\{\Delta_{\lambda'}(\overline{\Phi}^{\eta}\,\Delta\overline{p}^{\lambda'}u'd)+\Delta_{\varphi'}(\overline{\Phi}^{\eta}\,\Delta\overline{p}^{\varphi'}v'd) -\overline{\Phi}^{\eta}[\,\Delta_{\lambda'}(\Delta\overline{p}^{\lambda'}u'd)+\Delta_{\varphi'}(\Delta\overline{p}^{\varphi'}v'd)]\}_k\,.$$

The first two terms in the curly brackets give zero contribution if the summation is performed over a closed domain, or a domain with cyclic boundary conditions. Thus,

$$E_3=\Sigma_T\ (2/3)\ (\Delta A/g)\ \overline{\Phi}^{\eta}/(2h_1h_2\Delta\lambda\Delta\varphi)$$
$$[\Delta_\lambda\cdot(\Delta\overline{p}^{\lambda'}u'd)+\Delta_\varphi\cdot(\Delta\overline{p}^{\varphi'}v'd)]_k\ . \qquad (12)$$

The contribution to the kinetic energy generation of the remaining part of the "2/3" term is given by

$$E_4=\Sigma_{\mathbf{v}}\ -(2/3)\ (\Delta A/g)$$
$$\{u/(2h_1\Delta\lambda)\ [\Delta\overline{p}^{\lambda'}(\overline{RT/\overline{p}^{\eta}}^{\lambda'})\Delta_\lambda\overline{p}^{\eta}+\Delta\overline{p}^{\varphi'}(\overline{RT/\overline{p}^{\eta}}^{\varphi'})\Delta_{-\varphi}\overline{p}^{\eta}]$$
$$+v/(2h_2\Delta\varphi)\ [\Delta\overline{p}^{\lambda'}(\overline{RT/\overline{p}^{\eta}}^{\lambda'})\Delta_\lambda\overline{p}^{\eta}-\Delta\overline{p}^{\varphi'}(\overline{RT/\overline{p}^{\eta}}^{\varphi'})\Delta_{-\varphi}\overline{p}^{\eta}]\}_k\ .$$

Similarly as before, replacing the summation over the **v** points by the summation over the T points, one finally obtaines

$$E_4=\Sigma_T\ -(2/3)\ (\Delta A/g)/(2h_1h_2\Delta\lambda\Delta\varphi)$$
$$[u'd\ \Delta\overline{p}^{\lambda'}(\overline{RT/\overline{p}^{\eta}}^{\lambda'})\Delta_\lambda\overline{p}^{\eta}+v'd\ \Delta\overline{p}^{\varphi'}(\overline{RT/\overline{p}^{\eta}}^{\varphi'})\Delta_\varphi\overline{p}^{\eta}]_k\ . \qquad (13)$$

Now we have reached the point at which the finite-difference approximation to the continuity equation has to be specified. Following Janjić (1984), we choose

$$\Delta W_k+\overline{\nabla}\cdot(\mathbf{v}_k\Delta p_k)=0\ . \qquad (14)$$

Here the horizontal divergence operator has the form

$$\overline{\nabla}\cdot(\mathbf{v}_k\Delta p_k)=1/(2h_1h_2\Delta\lambda\Delta\varphi)$$
$$\{(1/3)\ [\Delta_\lambda(uh_2\Delta\varphi\Delta\overline{p}^{\lambda})+\Delta_\varphi(vh_1\Delta\lambda\Delta\overline{p}^{\varphi})] \qquad (15)$$
$$+(2/3)\ [\Delta_{\lambda'}(u'd\ \Delta\overline{p}^{\lambda'})+\Delta_{\varphi'}(v'd\ \Delta\overline{p}^{\varphi'})]\}_k\ ,$$

and W, defined at the interfaces of the η layers, is the finite-difference analogue of $\partial p/\partial t+\dot{\eta}\partial p/\partial \eta$.

Having defined the continuity equation approximation (15), from (9), (12), and (14)

$$E_1+E_3=\Sigma_T-(\Delta A/g)\,\overline{\Phi_k}^{\eta}\,\Delta W_k\,.$$

If we define the vertical averages of geopotential by

$$\overline{\Phi_k}^{\eta}=L_k\Phi_{k+1/2}+H_k\Phi_{k-1/2}\,,$$

where the half-level values are carried at the interfaces of the η layers, and

$$L_k+H_k=1\,,$$

after rearrangement,

$$E_1+E_3=\Sigma_T-(\Delta A/g)\,[(\Phi_{k+1/2}W_{k+1/2}-\Phi_{k-1/2}W_{k-1/2}) - \Delta\Phi_k(H_kW_{k+1/2}+L_kW_{k-1/2})\,. \tag{16}$$

After summation with respect to the vertical index, the contribution of the first term in the square brackets on the right hand side of (16) takes the form

$$\Sigma p_s\Phi_s\partial p_s/\partial t\,.$$

Here the summation is performed over all pressure points at the ground surface. This term should remain uncompensated by the $\omega\alpha$ term and therefore does not require further attention at this time.

Inspection of the remaining part of (16) reveals that it represents an approximation to the integral with respect to mass of the expression $-\alpha(\partial p/\partial t+\dot{\eta}\partial p/\partial\eta)_k$. Thus, the scheme

$$-(\Delta\Phi_k/c_p\Delta p_k)\,(H_k W_{k+1/2} + L_k W_{k-1/2})\,, \qquad (17)$$

which is a consistent approximation to $(\alpha/c_p)(\partial p/\partial t+\dot{\eta}\partial p/\partial\eta)_k$, after being multiplied by $c_p\Delta m=c_p\Delta p_k\Delta A/g$, and summed up over the T points in the free atmosphere, will compensate exactly the considered part of E_1+E_3.

Similarly, the sum of (10) and (13) represents an approximation to the integral with respect to mass of the expression $-\alpha\,\mathbf{v}_k\cdot\nabla p_k$. In the same way as in the case of (17), one finds that the approximation to $(\alpha/c_p)\,\mathbf{v}_k\cdot\nabla p_k$ of the form

$$\begin{aligned}
&1/(c_p 2h_1h_2\Delta\lambda\Delta\varphi\Delta p_k)\\
&\Big\{(1/3)\,uh_2\Delta\varphi\;\Delta\overline{p}^{\lambda}\Big[\big(RT/\overline{p}^{\eta}\big)\Delta_{\lambda}\overline{p}^{\eta}+\big(\overline{RT/\overline{p}^{\eta}}^{\lambda'\varphi'}\big)\Delta_{-\varphi}\overline{p}^{\eta}\Big]\\
&+(1/3)\,vh_1\Delta\lambda\;\Delta\overline{p}^{\varphi}\Big[\big(\overline{RT/\overline{p}^{\eta}}^{\lambda'\varphi'}\big)\Delta_{\lambda}\overline{p}^{\eta}-\big(\overline{RT/\overline{p}^{\eta}}^{\lambda'\varphi'}\big)\Delta_{-\varphi}\overline{p}^{\eta}\Big]\\
&+(2/3)\Big[u'd\;\Delta\overline{p}^{\lambda'}\big(\overline{RT/\overline{p}^{\eta}}^{\lambda'}\big)\Delta_{\lambda}\overline{p}^{\eta}+v'd\;\Delta\overline{p}^{\varphi'}\big(\overline{RT/\overline{p}^{\eta}}^{\varphi'}\big)\Delta_{\varphi}\overline{p}^{\eta}\Big]\Big\}_k\,,
\end{aligned} \qquad (18)$$

after being multiplied by $c_p\Delta m=c_p\Delta p_k\Delta A/g$, and summed up over the T points in the free atmosphere, will compensate exactly the contributions of E_2 and E_4. Thus, (17) and (18) are the energy conserving scheme for the $\omega\alpha$ term that we have been looking for.

In the pressure advection scheme in (18), we recognize the four horizontal fluxes appearing in the Arakawa type schemes. However, this scheme is not identical to the other advection schemes used in the model because of different averaging operators applied to define the values of (RT/p) in between the mass points.

5. RESULTS OF THE STEP-MOUNTAIN EXPERIMENTS

Genoa cyclogenesis, sigma/eta experiments. For initial testing of the step-mountain approach two out of the four Genoa cyclogenesis cases of Mesinger and Strickler (1982) have been chosen. These have been the two cases, from December 1969 and April 1973, for which the mountain/no mountain experiments have shown that mountains are necessary for cyclogenesis. Experiments were performed using the same integration region and the horizontal grid, consisting of 101×37 points (carrying the same variable), located at every other intersection of a 0.75×0.50 deg longitude×latitude mesh.

As this is of an obvious interest, the model code was written so as to have available the option of being run as an "eta" and as a sigma system model. The changes the model contained in its sigma "mode" compared to the model used by Mesinger and Strickler (1982) have been summarized in a previous paper (Mesinger, 1985). They include a change to a straightforward finite-difference hydrostatic equation, and to the Janjić (1984) horizontal advection schemes.

The previous paper contains also a description of the procedure which has been developed to construct mountains used for the experiments. One step of that procedure, as already mentioned in the preceding section as well as in the paper by Mesinger and Collins in these volumes, was the grouping of terrain points in order to achieve the same elevation values for each group of four neighboring height points. Mountains obtained as a result, for our "European" (Genoa cyclogenesis) region, are shown in Fig. 8. It may be noted that the terrain height contours shown in the figure are obtained using a code that involves a standard space interpolation scheme resulting in some

deformation and shifting of lines relative to their actual position. Without this shifting, the three contours printed would have touched at the southernmost tip of model Alps, where the eta model terrain heights form a vertical edge rising from sea level through all three of the lowermost model layers, that is, up to the height of 2433 m.

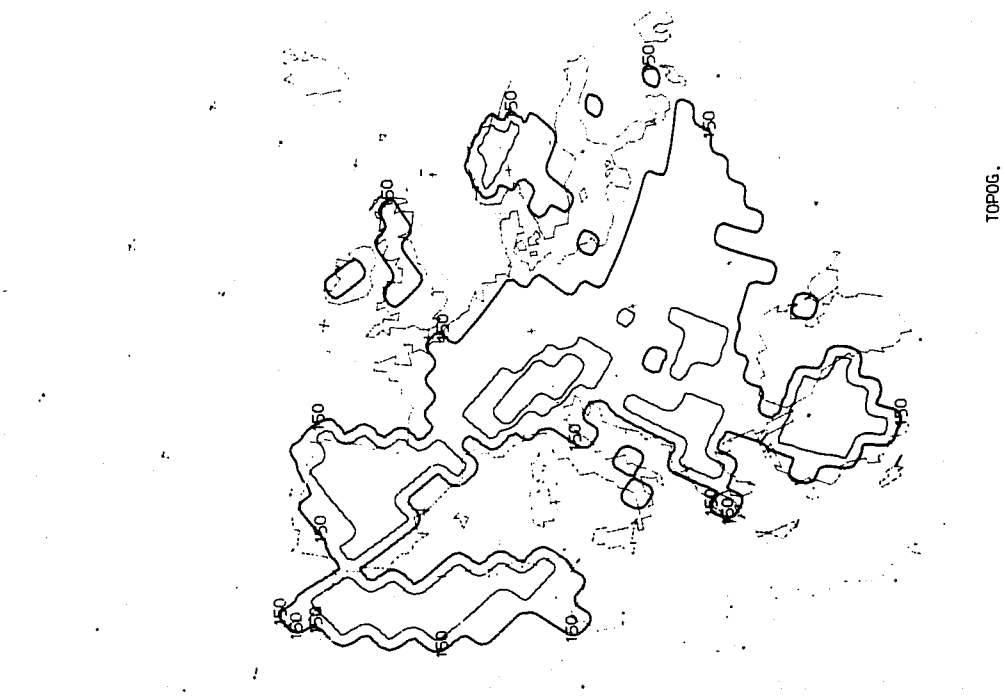

Fig. 8. Terrain heights used for the "European region" experiments. Steps at 290, 1112 and 2433 m are shown with contours at 150, 950 and 1750 m.

Experiments on both the December as well as the April case have been performed as well as analyzed from the verification point of view, and also from that of the differences between the eta and the sigma mode simulations. For the December case, both of these aspects have been covered by the 1985 paper. In a 48 h integration, starting from the same initial condition, the eta simulation has been in a number of ways more realistic than the previous sigma system simulation of Mesinger and Strickler. Of more interest, however, is the

comparison of the sigma against the eta simulation done using the same code. This comparison has revealed a higher level of noise of the sigma simulation. At all of the output maps inspected, 300, 500, 700 mb and the sea level, sigma mode maps were noisier than the eta mode maps. The difference is particularly striking at the 300 mb level, as can be seen on maps reproduced here as Fig. 9. In this figure, geopotential height maps are shown as upper panels, and temperature maps as lower panels. Both the height and the temperature field of the sigma mode simulation (left hand panels) are visibly noisier than the corresponding fields of the eta mode simulation (right hand panels).

A maximum intensity near the tropopause level of the noise generated in the sigma system presumably due to the pressure gradient force error is consistent with the present understanding of this error, as summarized in earlier sections. Specifically, at the uppermost of the three levels considered, the lapse rate would be expected, at most places, to change more with height than at the other two levels, resulting in larger pressure gradient force errors.

Published reports on eta simulations of the Buzzi-Tibaldi April 1973 case (Mesinger, 1985; Mesinger and Pierrehumbert, 1986) address the verification aspect only. Starting the integration with the initial conditions of the same time as that of the initial analyses published by Buzzi and Tibaldi (1978), 12 GMT 2 April, a rather realistic 36 h simulation was achieved. An approximately correct depth of the lee cyclone in this simulation was a visible improvement over the earlier 24 h simulation of Bleck (1977) verifying at the same time, shown in his Fig. 11. In view of difficulties encountered in previous simulations of Genoa lee cyclogenesis (Bleck, 1977; Mesinger and Strickler, 1982; Dell'Osso and Radinovic, 1984), the cutoff obtained on the 500 mb geopotential height map was parhaps a particularly encouraging feature.

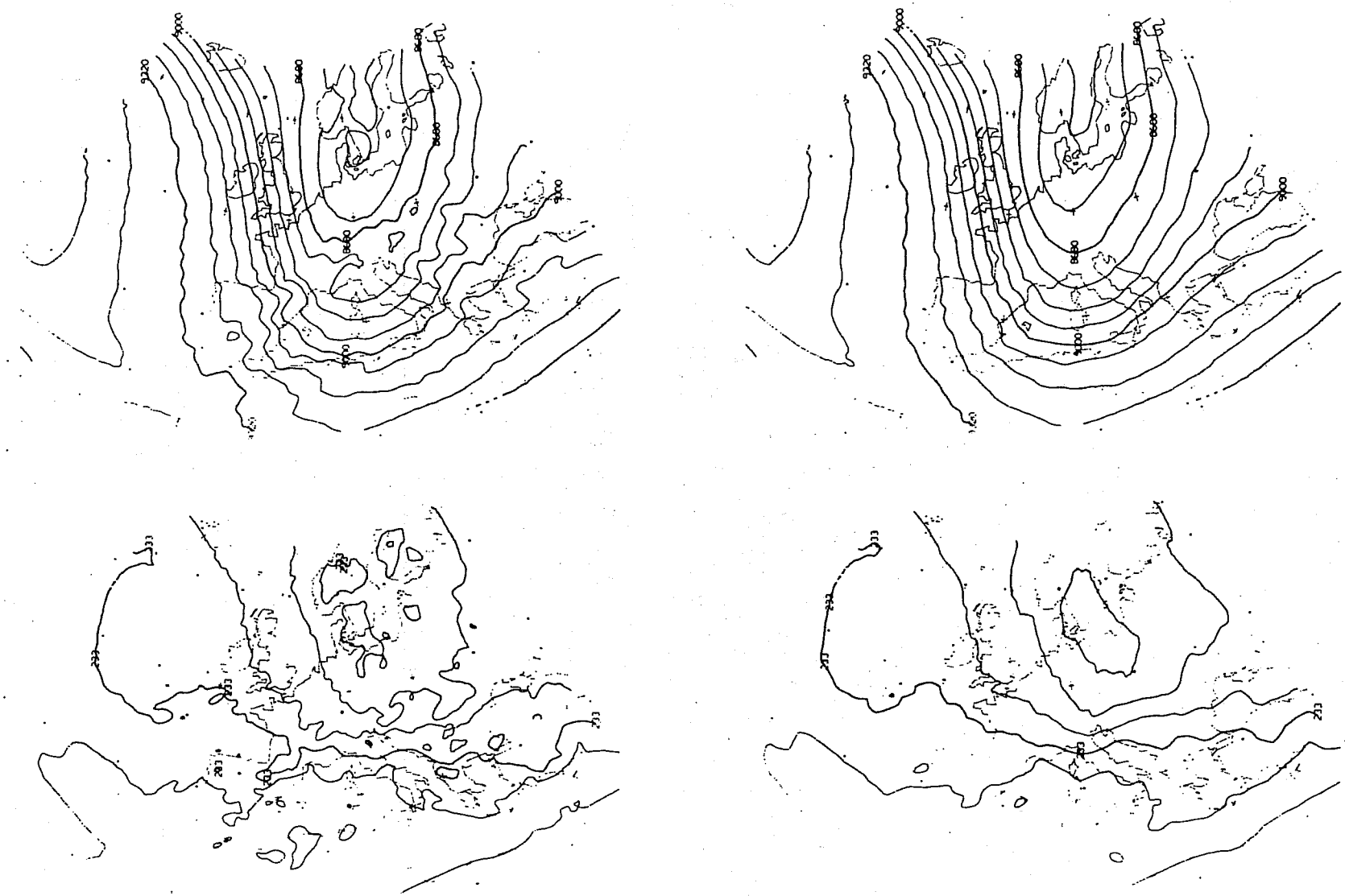

Fig. 9. 300 mb geopotential heights (upper panels) and temperatures (lower panels) obtained in 48 h simulations using the sigma system (left hand panels) and the eta system (right hand panels). Contour interval is 80 m for geopotential height, and 2.5 K for temperature.

Fig. 10. Sea level pressure maps obtained in 36 h simulations using the sigma system (left hand panel) and the eta system (right hand panel), verifying at 00 GMT 4 April 1973. Contour interval is 2.5 mb; see text for other details.

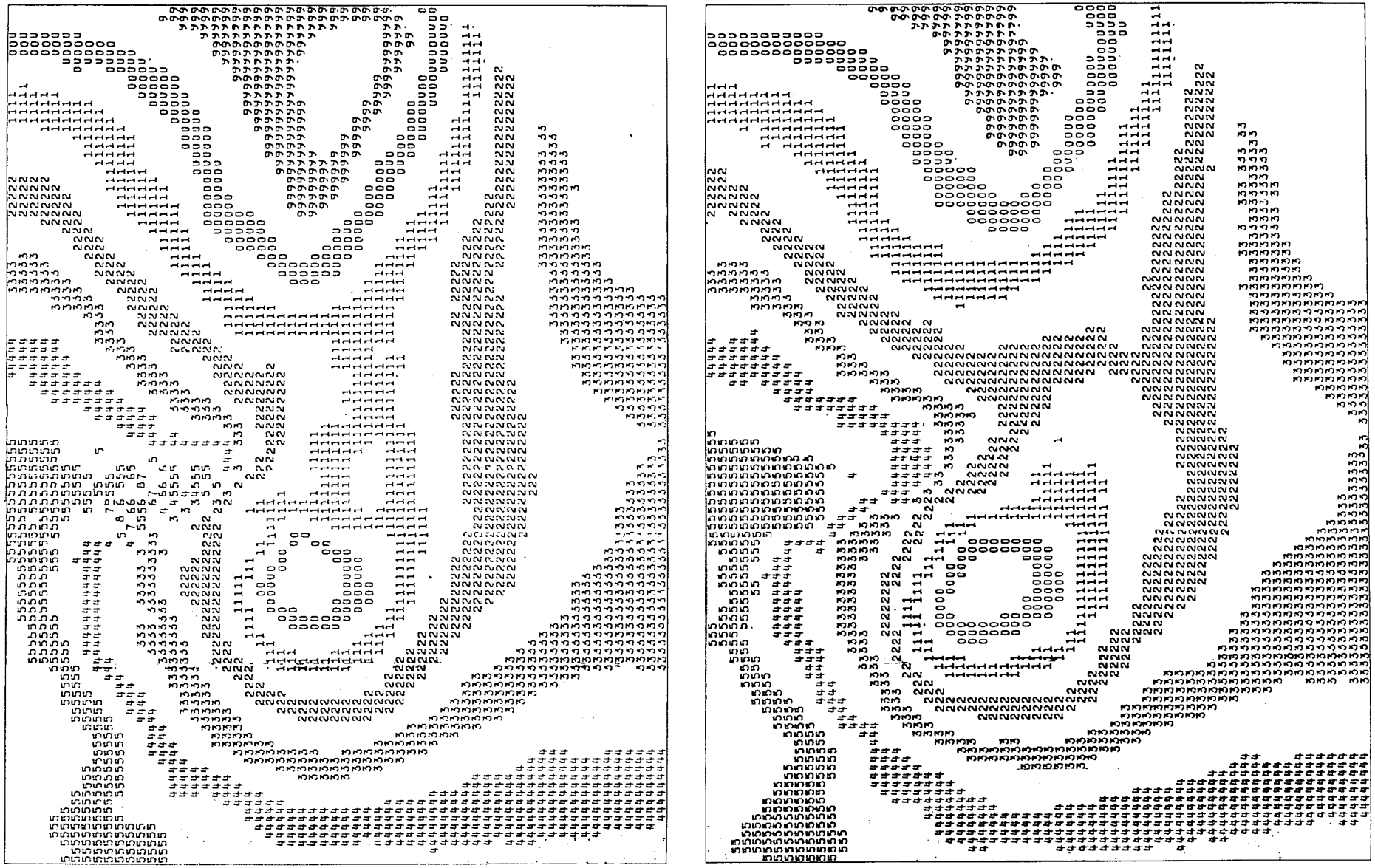

Fig. 11. 850 mb geopotential height maps obtained in 36 h simulations using the sigma system (left hand panel) and the eta system (right hand panel), verifying at 00 GMT 4 April 1973. Contour interval is 20 m; see text for other details.

Subsequently, an eta/sigma mode experiment was performed also on the April 1973 case, but, unfortunatelly, no contour maps are available for the sigma mode run. Therefore, in Figs. 10 and 11, line printer maps are shown, for both the sigma and the eta mode run. For more detail in the area of interest, only sections of the two maps are shown. The experiment has been performed with model parameters same as for the preceding figure, except that the horizontal diffusion, found to be of no practical consequence with the coefficient chosen, was absent. In Fig. 10 sections of the sea level pressure maps are shown. For these maps, contour interval is 2.5 mb, with the 1000 mb isobar running along the edge of the area of zeros facing the neighboring area of nines. Continent outlines can be inferred by comparison of the two isobars which are common for the line printer eta mode map, right hand panel, and for the contour map shown as the left hand panel in Fig. 8 of Mesinger (1985). These are the 1000 mb isobar, as well as that of 1020 mb, in the line printer maps running along the edge of the area of fours, and facing the neighboring area of threes.

An insufficiently deep lee cyclone is seen on the sigma mode map, left hand panel, by about one contour interval. While there is no difference in ridging north of the lee cyclone in terms of isobars that are cut off, one can note that on the side of the advancing cold air all of the isobars of the eta mode map have generally progressed further to the east than the corresponding isobars on the sigma mode map. Note, in particular, the 1010 and 1012.5 mb isobars, on the two sides of the area of twos. Thus, there is evidence of an intensified flow around the Alpine barrier. Finally, the sigma mode map is noisier that the eta mode map. The difference is particularly visible in the area of the Alps, in which the higher temperature noise of the sigma mode run results in very erratic fictitious sea level pressure values. Recall that model parameters provide for no horizontal smoothing or lateral diffusion to reduce the noise as customarily would have been done.

In Fig. 11 geopotential height contours of the 850 mb surface are shown. Contour interval is 20 m, and the "reference" contour, along the side of zeros and facing the neighboring nines, is 1320 m. The lee cyclone of the sigma mode map, left hand panel, and that of the eta mode map, right hand panel, are at this level of about the same depth. As there is no appreciable vertical tilt of the axis of the low in the considered layer, the eta mode cyclone is seen to be warmer than the sigma mode cyclone. Ridging of the trough axis north of the lee cyclone is at this level more intensive in the eta mode run, which represents an improvement according to observations. Finally, the noisiness of the sigma mode run compared to the eta mode run is more pronounced than at the sea level.

There is not much difference, however, in the progress of the cutoff at the 500 mb level (not shown). Thus, the success in simulation of the mid-tropospheric cutoff did not come as a result of the step-mountain method. We are of the opinion, therefore, that simulation of the cutoff in this case was successful simply as a result of the generally high accuracy of the simulation of the ridging in the lower troposphere north of the Alps, both in the eta as well as in the sigma mode run. As in the December 1969 case, the noisiness of the sigma mode run increases with height, and becomes substantial at the mid and upper troposphere; about as illustrated by maps of Fig. 9.

The Appalachian redevelopment experiment. Another region used to test the performance of the step-mountain system was a "North American" region (Mesinger and Deaven; in Mesinger et al., 1987). The objective of the North American region experiments was a comparison against the performance of another model with roughly the same computational effort in terms of the integration region as well as the space resolution. For convenience, U.S. National Meteorological Center's Nested Grid Model was chosen for that

purpose. Therefore, grid parameteres for the North American region were chosen so as to mimic those of the NGM. This is a triply nested model, with about one third of the computational effort spent on two outermost grids. Its grid length on the innermost grid, defined on stereographic projection, is 91 km at 60°N. With no nesting, to account for the overhead due to the NGM's outer grids,Mesinger and Deaven have chosen a region resulting from about the same grid distance, and the number of grid points roughly 25 percent higher than that of the NGM's innermost grid. As our code, for efficiency and for a more uniform grid geometry, is written in terms of rotated spherical coordinates (Undén, 1980; Bates and McDonald, 1982; for transformation equations, see Mesinger, 1971), we have positioned our grid by choosing the location of its central (height) point; the coordinates chosen were the longitude of 100°W, and the latitude of 52.5°N. The model region was defined to span 75×70 deg of (transformed) longitude×latitude, with grid points at every other intersection of the (15/26)×(14/26) deg transformed longitude×latitude mesh. Thus, the horizontal grid consisted of 8581 height points and 8580 velocity points; about 1.246 times the number of grid points of the NGM's innermost horizontal grid. The choices made resulted in a grid distance varying from 79.6 km at the model's southern and northern boundary, to 87.7 km at its central grid line. Also, this made for a region along the model's central meridian extending from 17.5°N to 87.5°N (actual) latitude.

For initial North American region experiments, Mesinger and Deaven have used the GFDL 9-layer vertical structure, same as that of the European region simulations of the preceding subsection. For these initial experiments, for convenience, step-mountains were derived from the terrain fields used for the NMC rhomboidal-40 spectral prediction model. Forecasts of this same model were used to prepare the step-mountain model lateral boundary conditions.

Of the so-called "special cases" (Collins and Tracton, 1985) which have been used for comparison of the performance of NGM against that of the NMC Limited-Area Forecast Model (LFM) as "historical cases of meteorological importance", Mesinger and Deaven have looked for cases in which dynamics seemed as primary or at least a possibly important factor in governing the processes that have attracted interest. In this way, "Case 2", and subsequently "Case 1" have been chosen. For "Case 2", described by Collins and Tracton as "dramatic cold air plunge into the deep south", NGM forecast was subjectively ranked as "much better" than the LFM forecast. Result of the 24 h step-mountain model forecast was subjectively judged as similar to the NGM forecast and will not be shown here.

"Case 1" may perhaps not look like a good candidate for tests of the presently available (dry) step-mountain model since it was chosen for NGM/LFM comparison primarily as responsible for severe weather associated with a series of tornadoes causing many deaths and injuries, followed by spring snowstorms across the Northeast. The initial time of this case was 00 GMT 28 March 1984. At that time a perturbation-like low is centered in Texas on a frontal line running further east roughly along the Gulf Coast. As the cyclone moves eastward it develops a new center to the southeast of the original center. This double structure is seen on the NMC surface analysis for 00 GMT 29 March, shown in Fig. 12. After 03 GMT the original center, west of the Appalachians in the figure, disappears while the eastern center deepens setting some low barometric records and resulting in up to 75 cm of snow across interior sections of Pennsylvania, New York and New England. NGM forecast for this case was ranked as "better" than LFM. However, same as LFM, it did not show the redevelopment in Georgia. Therefore, nine additional forecasts were made by Collins and Tracton to test the sensitivity of the forecast to various factors; one of them was a "silhouette terrain" forecast, differing from control

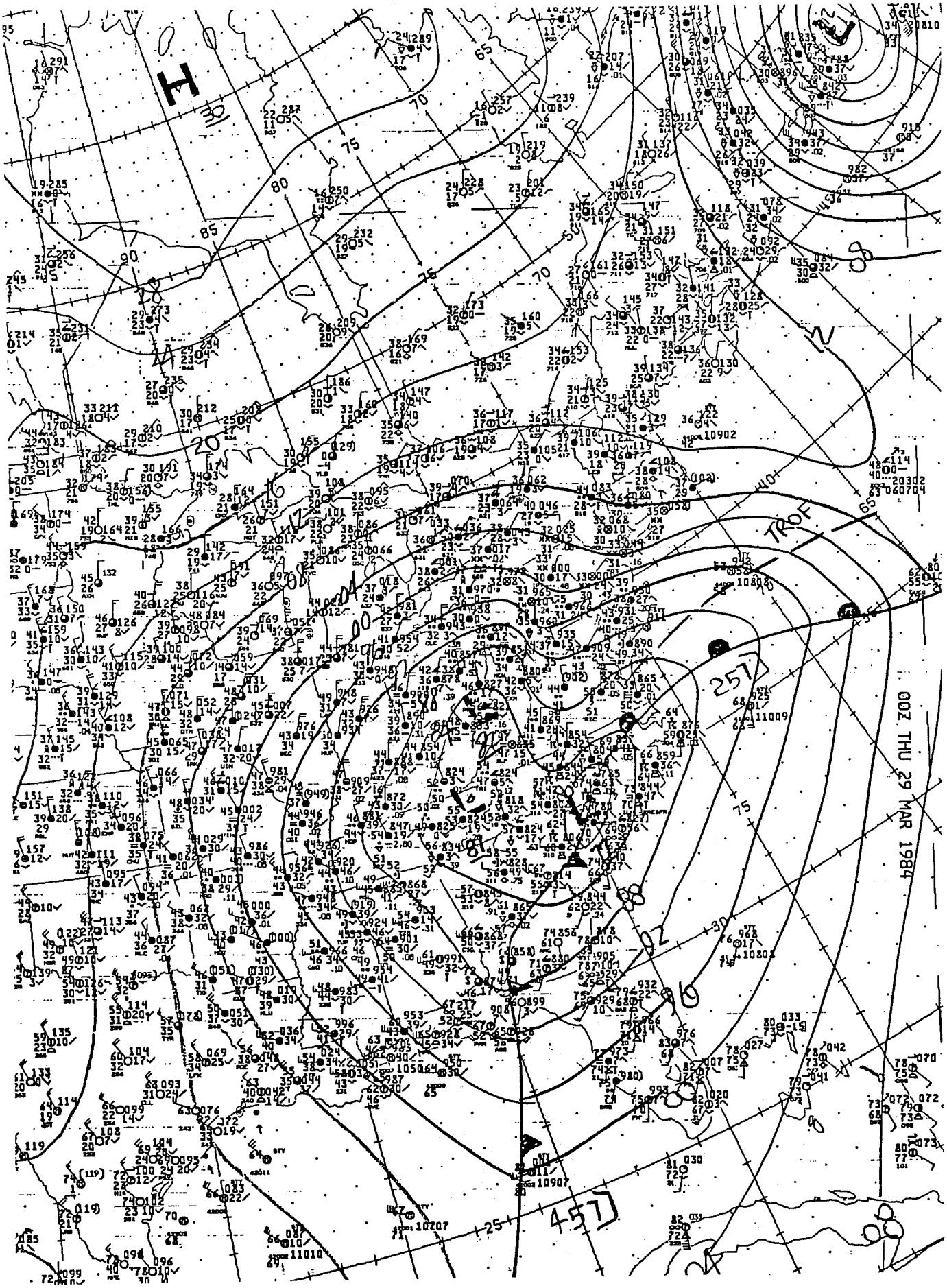

Fig. 12. Section of the U.S. National Weather Service surface map for 00 GMT 29 March 1984.

by using the NGM version of silhouette mountains (Hoke et al., 1985). None of the nine sensitivity runs showed indication of the redevelopment.

The same case was studied also by Kocin et al. (1984). In spite of a 47 km grid distance and a 12 hour later starting time of their integrations, their results do not show an obvious improvement over those of Collins and Tracton.

The 24 h step-mountain forecast for this case, with model parameters as described, was judged to be of about the same quality as that of various NGM runs. There was no indication of the redevelopment: the low, centered in northwestern tip of Georgia, had inner isobars of a circular shape, with hardly any signs of ridging on its northeastern side.

A sensitivity experiment was performed with model parameters the same as used for this forecast, except that the vertical resolution and distribution of model layers was changed to that of the 16-layer NGM structure. A section of the sea level pressure and 1000-500 mb thickness map obtained as a result of this experiment is shown in Fig. 13. In comparison with results of the 9-layer run, the ridging seen to the northeast of the center represents a clear hint of redevelopment, more so than can be seen in any of the nine NGM sensitivity experiments.

Since in view of the eta-coordinate mountain derivation procedure the change in vertical resolution has necessarily involved a change in model mountains - perhaps an increase in the height of Appalachians - the question has in this way arisen as to whether the increased vertical resolution or the changed mountains were primarily responsible for the resulting ridging. Therefore, hoping to discriminate between these two possibilities, an experiment was performed in which the "spectral" mountains as input for the derivation of the

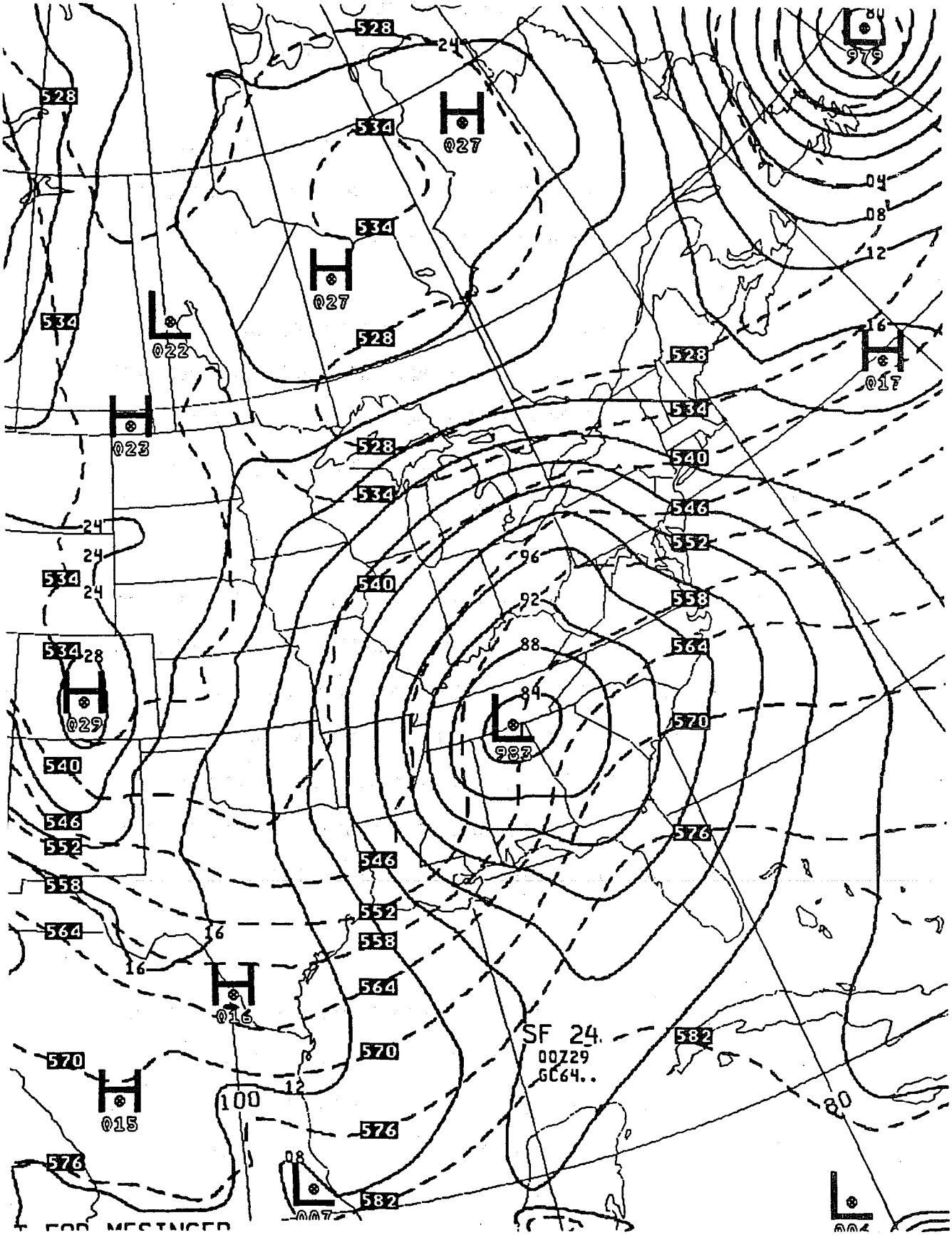

Fig. 13. Section of a 24 h simulation of sea level pressure (full lines) and 1000-500 mb thickness (dashed lines), using terrain derived from NMC "spectral" mountains, and verifying at 00 GMT 29 March 1984.

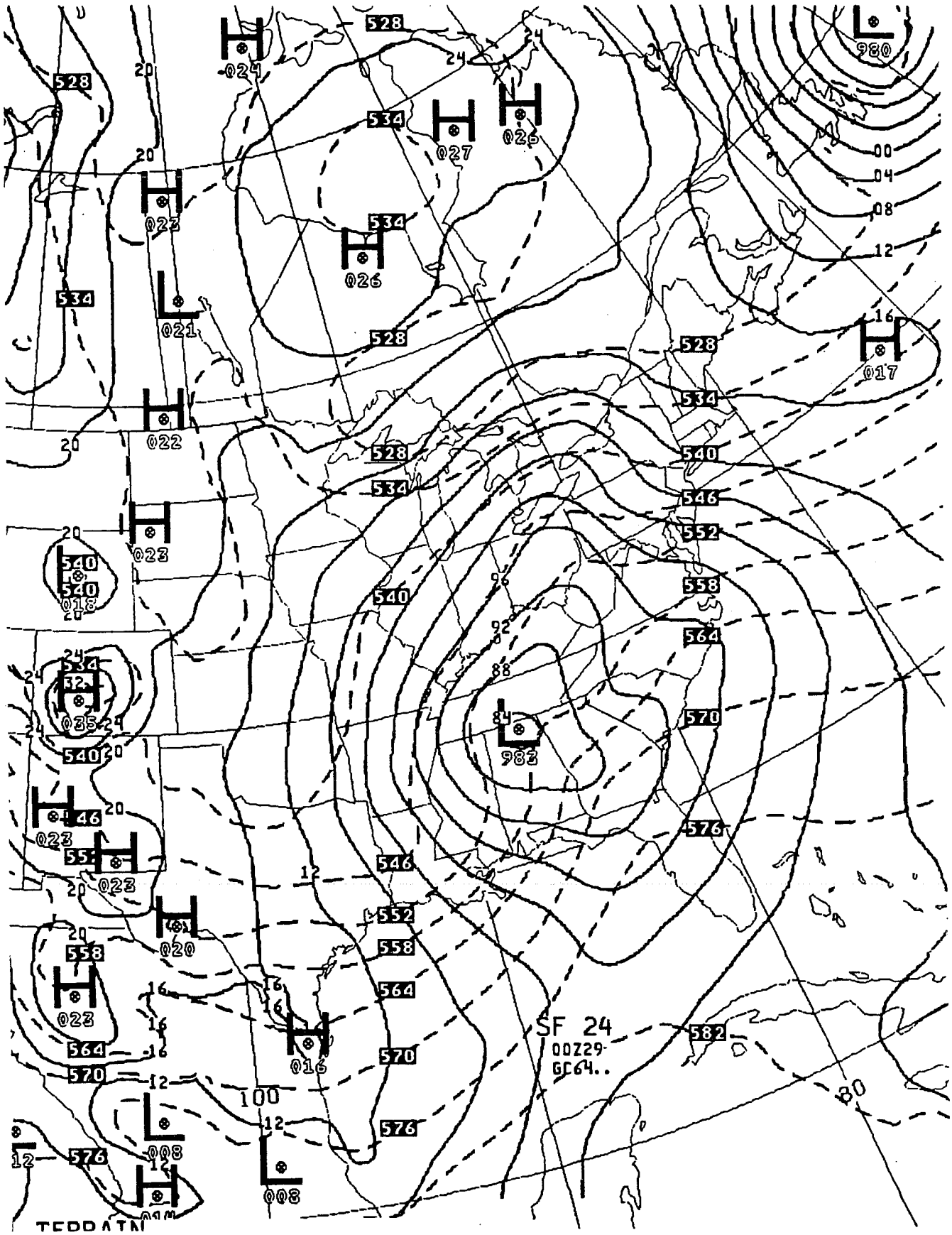

Fig. 14. Section of a 24 h simulation of sea level pressure (full lines) and 1000-500 mb thickness (dashed lines), using terrain derived from NMC "silhouette" mountains, and verifying at 00 GMT 29 March 1984.

step-mountain terrain were replaced by the mentioned NGM "silhouette" mountains. The result of this experiment is shown in Fig. 14. A very much increased intensity of the ridging can be seen, with a clear indication of the redevelopment over Georgia and South Carolina.

One may still wonder to what extent the success in the simulation of the (presumably) "trigger" stage of redevelopment east of Appalachian Mountains came as a result of the numerical technique employed, and to what extent it is simply a result of higher mountains. In this connection it should be recalled that in mentioned experiments with the NGM model the use of higher mountains (Run 6, Fig. 11 in Collins and Tracton, 1985) in no way gave a result which was superior to the general level of the remaining nine (including control) runs. Thus, a substantial difference in the ability of the two models to show sensitivity to the effect of higher mountains has apparently been identified, and this difference can only be explained as a result of the difference in numerical schemes of the two models.

6. CODE EFFICIENCY

An important problem is a possible loss in efficiency of the code allowing for internal boundaries compared to the code of the standard sigma system model. In view of the material of the two preceding sections a related question is that of vectorization when using the horizontal E grid. Namely, if on the E grid the horizontal indices are defined in a straightforward manner, the indices of the grid points surrounding the point at which the calculation is performed cannot be calculated by simply adding or subtracting a constant increment. For the same pattern of grid points, the increment will depend on whether the indices of the reference point are even or odd. Thus, code efficiency on vector machines may be reduced. A possible solution pointed out by Janjić and Mesinger (1984, p. 62) was suitable for hemispheric or global models only.

In our code, the internal boundary problem is solved by defining masks which are set to zero underneath the topography and to one otherwise. In this way exactly the same arithmetic operations are performed at all grid points, no matter whether they are in the atmosphere or under the ground. The same method is used to distinguish between land and sea.

As in the case of the internal boundaries, in order to provide different treatment along the lateral boundaries of the integration domain, the masks consisting of zeros and ones are used.

To eliminate the indexing problem arising due to the structure of the E grid, a one-dimensional horizontal indexing was devised, as schematically represented in Fig. 15. As indicated in the example shown in the figure, the one-dimensional index K increases row-wise from left to right, and, reaching the right end of a row, jumps to the left end of the next row above. The

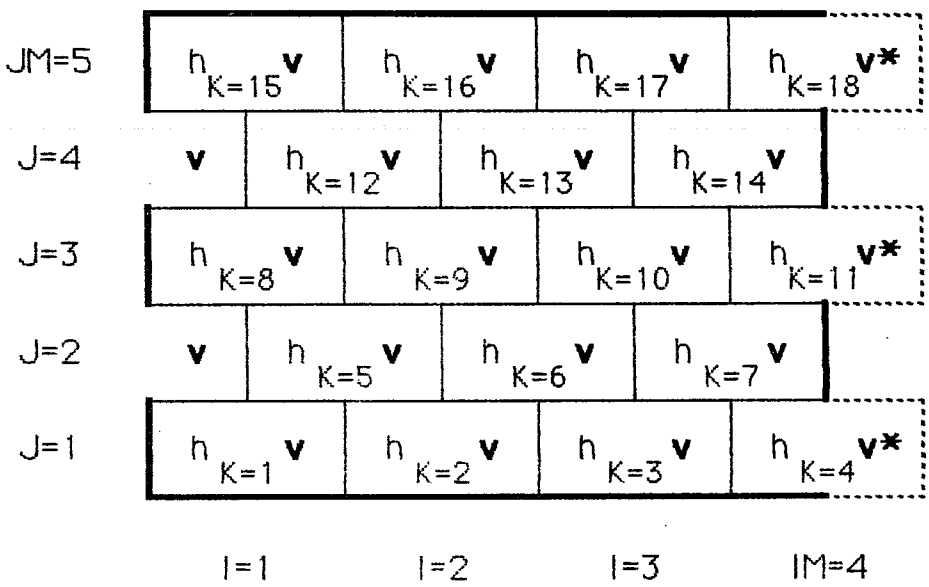

Fig. 15. Schematic representation of efficient one-dimensional indexing on the E grid suitable for both limited area as well as hemispheric/global area integrations. See text for additional details.

velocity points equipped with asterisks at the right ends of the rows with odd values of the two-dimensional latitudinal index J have the same value of the one-dimensional index K as the height points to the left of them, but are actually located at the left end of the next row above.

With this indexing, the horizontal indices of the grid points surrounding the point at which the calculation is performed are easily calculated adding constant increments. This makes coding straightforward, and the resulting code easily readable. An additional advantage of the one-dimensional horizontal indexing is the large arrays processed in the innermost loops, which on some vector computers results in faster computations.

In order to ensure easy portability, the vector code was written following with only a single exception the standard ANSI FORTRAN 77. The single exception was the CYBER 205 half precision extension using 32 bit word internal representation.

The full-precision vector code was faster than the original scalar code more than ten times, and with the half-precision extension, this factor was increased to over fifteen. A comparison with a very carefully designed vector code used operationally shows that the efficiency standard required in an operational environment has been achieved although no special vector machine extensions were used.

7. CONCLUDING DISCUSSION

The techniques related to the representation of mountains were in this lecture considered from the point of view of grid point models. The pressure gradient force error problem was reexamined, taking our Seminar 1983 lecture as the starting point. Error calculations have been performed for three additional

schemes, and for three temperature profiles. Generally rather large values of errors have been obtained, with no obvious tendency for errors to reduce with increasing vertical resolution.

Other problems of the terrain-following coordinates are known; recently, perhaps unexpected sensitivity to the formulation of the lateral diffusion on sigma vs. that on pressure surfaces has been identified. Both the pressure gradient force problem, as well as the diffusion problem, are for the most part eliminated by using vertical interpolation and simulated vertical interpolation schemes. This, however, goes against the simplicity of the sigma system. In addition, the possibility of residual errors of the type mentioned by Sadourny et al. (1981) cannot be ruled out.

Technical problems of one of the alternative approaches, that of the step-mountain (eta) system, have been considered in some detail. For an advection scheme achieving a strict control of the nonlinear energy cascade on the semi-staggered E grid, it is demonstrated that a straightforward no-slip wall boundary condition maintains conservation properties of the scheme with no vertical walls which control this energy cascade from large to small scales. However, with that simple boundary condition considered, momentum is not conserved. The technique for achieving mass conservation in the scheme for prevention of the two-grid-interval noise, and the scheme for calculation of the potential to kinetic energy conversion, in the two-dimensional case, are presented. Thus, very few difficulties are encountered in maintaining the favorable features of schemes of a carefully designed sigma system model.

Using the code which can be run either as a sigma or as the step-mountain model, the effects of the errors inherent to the sigma system have been demonstrated in real data runs. Namely, in two parallel integrations performed

with the same model code and same other model parameters, the sigma system runs showed increased noisiness, particularly in temperature fields at higher levels. One may speculate that this noise is related to the sigma system pressure gradient force error. Namely, the mass field may have been forced to adjust to the erroneous wind field produced by the false pressure gradient force. In any case, this remains a problem which requires further investigation.

In numerical simulations performed, the eta coordinate model has shown considerable skill, both in relative and absolute terms. It has performed better than its sigma coordinate version in both parallel runs. The forecasts produced by the eta model have shown high degree of realism and can be considered successful from the synoptic point of view. In a situation of a particular interest, that of the redevelopment east of Appalachian Mountains, it has shown ability to forecast the onset stage of the phenomenon. This ability was lacking in another model of about the same horizontal and vertical resolution.

In contrast to what perhaps may be expected, it has also been demonstrated that the eta cooordinate model code can, and has been, easily vectorized in the most straightforward manner.

We believe that the results summarized and/or shown here demonstrate that the eta coordinate is not only competitive, but has visible advantages compared to the presently almost exclusively used sigma coordinate. Interest remains strong in using and developing isentropic coordinate models. While being technically perhaps more complex than the eta system, this certainly is another approach which offers a number of benefits over the sigma system, including one would expect that of the pressure gradient force error.

Acknowledgments. Part of the work reported here has been done while the two of us of have enjoyed the hospitality of the U.S. National Meteorological Center. It is a pleasure for us to acknowledge the support and encouragement of Dr. William Bonner, Director; and of Dr. John A. Brown, Jr., Head of the Development Division of the Center, in which the work has been performed.

Many useful suggestions on sections of the manuscript have been made by Dr. Bruce Ross, of the Mesoscale Dynamics Group of the Geophysical Fluid Dynamics Laboratory, Princeton University.

References

Arakawa, A., 1972: Design of the UCLA general circulation model. *Numerical Simulation of Weather and Climate*, Tech. Rep. No. 7, Dept. Meteor., UCLA, Los Angeles.

Arakawa, A., and V. R. Lamb, 1977: Computational design of the basic dynamical processes of the UCLA general circulation model. *Methods in Computational Physics*, Vol. 17, Academic Press, 173-265.

Arakawa, A., and M. J. Suarez, 1983: Vertical differencing of the primitive equations in sigma coordinates. Mon. Wea. Rev., **111**, 34-45.

Bates, J. R., and A. McDonald, 1982: Multiply-upstream, semi-Lagrangian advective schemes: Analysis and application to a multi-level primitive equation model. *Mon. Wea. Rev.*, **110**, 1831-1842.

Bleck, R., 1977: Numerical simulation of lee cyclognesis in the Gulf of Genoa. *Mon. Wea. Rev.*, **105**, 428-445.

Brown, J. A., 1974: On vertical differencing in the σ-system. Office Note 92, National Meteorological Center, NWS/NOAA, 13 pp.

Burridge, D., and J. Haseler, 1977: A model for medium range weather forecasting: adiabatic formulation. Tech. Rep. No. 4, ECMWF, Reading, U.K., 46 pp.

Buzzi, A., and S. Tibaldi, 1978: Cyclogenesis in the lee of the Alps: A case study. *Quart. J. Roy. Meteor. Soc.*, **104**, 271-287.

Collins, W. G., and M. S. Tracton, 1985: Evaluation of NMC's regional analysis and forecast system - heavy precipitation events. *Preprints, Sixth Conf. Hydrometeorology*, Indianopolis, Amer. Meteor. Soc.

Corby, G. A., A. Gilchrist and R. L. Newson, 1972: A general circulation model of the atmosphere suitable for long period integrations. *Quart. J. Roy. Meteor. Soc.*, **98**, 809-832.

Cullen, M. J. P., 1983: Current progress and prospects in numerical techniques for weather prediction models. *J. Comp. Phys.*, **50**, 1-37.

Cullen, M. J. P., 1985: Developments in global modelling at the U.K. Meteorological Office. GARP Special Rep., No. 43, WMO, Geneva, I, 83-98.

Dell'Osso, L., and Dj. Radinovic, 1984: A case study of cyclone development in the lee of the Alps on 18 March 1982. *Contrib. Atmos. Phys.*, **57**, 369-379.

Gary, J. M., 1973: Estimate of truncation error in transformed coordinate, primitive equation atmospheric models. *J. Atmos. Sci.*, **30**, 223-233.

Hoke, J. E., N. A. Phillips, G. J. DiMego and D. G. Deaven, 1985: NMC's regional analysis and forecast system -- results from the first year of daily, real-time forecasting. *Preprints, Seventh Conf. Numerical Weather Prediction*, Montreal, Amer. Meteor. Soc., 444-451.

Janjic, Z. I., 1977: Pressure gradient force and advection scheme used for forecasting with steep and small scale topography. *Contrib. Atmos. Phys.*, **50**, 186-199.

Janjic, Z. I., 1979: Forward-backward scheme modified to prevent two-grid-interval noise and its application in sigma coordinate models. *Contrib. Atmos. Phys.*, **52**, 69-84.

Janjic, Z. I., 1984: Non-linear advection schemes and energy cascade on semi-staggered grids. *Mon. Wea. Rev.*, **112**, 1234-1245.

Janjic, Z. I., and F. Mesinger, 1984: Finite-difference methods for the shallow water equations on various horizontal grids. *Numerical Methods for Weather Prediction*, Seminar 1983, Vol. 1, ECMWF, Reading, U.K., 29-101.

JMA, 1986: Outline of Operational Numerical Weather Prediction at Japan Meteorological Agency. Japan Meteorological Agency, Tokyo, 94 pp.

Kocin, P. J., L. W. Uccellini, J. W. Zack and M. L. Kaplan, 1984: Recent examples of mesoscale numerical forecasts of severe weather events along the East Coast. NASA Tech. Memo. TM 86172, 57 pp.

Kurihara, Y., 1968: Note on finite difference expressions for the hydrostatic relation and pressure gradient force. *Mon. Wea. Rev.*, **96**, 654-656.

Mahrer, Y., 1984: An improved numerical approximation of the horizontal gradients in a terrain-following coordinate system. *Mon. Wea. Rev.*, **112**, 918-922.

Mattocks, C., and R. Bleck, 1986: Jet streak dynamics and geostrophic adjustment processes during the initial stages of lee cyclogenesis. *Mon. Wea. Rev.*, **114**, 2033-2056.

Mesinger, F., 1971: Numerical integration of the primitive equatins with a floating set of computation points: Experiments with a barotropic global model. *Mon. Wea. Rev.*, **99**, 15-29.

Mesinger, F., 1973: A method for construction of second-order accuracy difference schemes permitting no false two-grid-interval wave in the height field. *Tellus*, **25**, 444-458.

Mesinger, F., 1982: On the convergence and error problems of the calculation of the pressure gradient force in sigma coordinate models. *Geophys. Astrophys. Fluid Dyn.*, **19**, 105-117.

Mesinger, F., 1984: A blocking technique for representation of mountains in atmospheric models. *Riv. Meteor. Aeronautica*, **44**, 195-202.

Mesinger, F., 1985: The sigma system problem. *Preprints, Seventh Conf. Numerical Weather Prediction*, Montreal, Amer. Meteor. Soc., 340-347.

Mesinger, F., 1987: Some more calculations of the sigma system pressure gradient force errors. To be published.

Mesinger, F., and Z. I. Janjic, 1984: Finite-difference schemes for the pressure gradient force and for the hydrostatic equation. *Numerical Methods for Weather Prediction*, Seminar 1983, Vol. 1, ECMWF, Reading, U.K., 103-157.

Mesinger, F., Z. I. Janjic, S. Nickovic, D. Gavrilov and D. G. Deaven, 1987: The step-mountain coordinate: model description, and performance for cases of Alpine lee cyclogenesis and for a case of an Appalachian redevelopment. Submitted to *Mon. Wea. Rev.*

Mesinger, F., and R. T. Pierrehumbert, 1986: Alpine lee cyclogenesis: numerical simulation and theory. GARP Publ. Ser., No. 27, Vol. I, WMO, Geneva, 141-163.

Mesinger, F., and R. F. Strickler, 1982: Effects of mountains on Genoa cyclogeneses. *J. Meteor. Soc. Japan*, **60**, 326-338.

Michaud, R., and R. Sadourny, 1986: Sensitivity of January 1983 SST experiments to the formulation of lateral diffusion. World Climate Programme, WCP-121, WMO, Geneva, 154-164.

Mihailovic, D. T., and Z. I. Janjic, 1986: Comparison of methods for reducing the error of the pressure gradient force in sigma coordinate models. *Meteor. Atmos. Phys.*, **35**, 177-184.

Miyakoda, K., 1973: Cumulative results of testing a meteorological-mathematical model. The description of the model. *Proc. Roy. Irish Acad.*, **73A**, 99-130.

Nakamura, H., 1978: Dynamical effects of mountains on the general circulation of the atmosphere. I: Development of finite-difference schemes suitable for incorporating mountains. *J. Meteor. Soc. Japan*, **56**, 317-340.

Phillips, N. A., 1957: A coordinate system having some special advantages for numerical forecasting. *J. Meteor.*, **14**, 184-185.

Phillips, N. A., 1973: Principles of large scale numerical weather prediction. *Dynamic Meteorology*, P. Morel, Ed., D. Reidel Publishing Co., Dordrecht, 1-96.

Phillips, N. A., 1974: Application of Arakawa's energy conserving layer model to operational numerical weather prediction. Office Note 104, National Meteorological Center, NWS/NOAA, 40 pp.

Rousseau, D., and H. L. Pham, 1971: Premiers résultats d'un modèle de prévision numérique à courte échéance sur l'Europe. *La Météorologie*, **20**, 1-12.

Sadourny, R., 1984: Entropy coordinate, quasi-geostrophic turbulence and the design of lateral diffusion in general circulation models. *Numerical Methods for Weather Prediction*, Seminar 1983, Vol. 1, ECMWF, Reading, U.K., 255-290.

Sadourny, R., 1985: Midlatitude systematic errors in numerical models. GARP Special Rep., No. 43, WMO, Geneva, III, 156-174.

Sadourny, R., O. P. Sharma, K. Laval and J. Canneti, 1981: Modelling of the vertical structure in sigma coordinate: a comparative test with FGGE data. Intern. Conf. on Prelim. FGGE Data Analysis and Results, Proceedings, WMO, Geneva, 294-302.

Sela, J. G., 1982: The NMC spectral model. NOAA Tech. Rep. NWS30, NWS/NOAA, Silver Spring, MD, 36 pp.

Simmons, A. J., and D. M. Burridge, 1981: An energy and angular-momentum conserving vertical finite-difference scheme and hybrid vertical coordinates. *Mon. Wea. Rev.*, **109**, 758-766.

Simmons, A. J., and M. Jarraud, 1984: The design and performance of the new ECMWF operational model. *Numerical Methods for Weather Prediction*, Seminar 1983, Vol. 2, ECMWF, Reading, U.K., 113-164.

Smagorinsky, J., J. L. Holloway, Jr., and G. D. Hembree, 1967: Prediction experiments with a general circulation model. Proc. Inter. Symp. Dynamics Large Scale Atmos. Processes, Nauka, Moscow, 70-134.

Sundqvist, H., 1979: Vertical coordinates and related discretization. GARP Publ. Ser., No. 17, Vol. II, WMO, Geneva, 1-50.

Tibaldi, S., 1986: Envelope orography and maintenance of quasi-stationary waves in the ECMWF model. *Advances in Geophysics*, (in press).

Tokioka, T., 1978: Some considerations on vertical differencing. *J. Meteor. Soc. Japan*, **56**, 98-111.

Tomine, K., and S. Abe, 1982: A trial to reduce truncation errors of the pressure gradient force in the sigma coordinate systems. *J. Meteor. Soc. Japan*, **60**, 709-716.

Undén, P., 1980: Changing the spherical grid for LAMs. *Limited Area Modeling, LAM Newsletter*, **1**, No. 1, pp. 12-16. [Available from SMHI, Box 923, Norrköping, Sweden].

WMO-ICSU, 1974: *Modelling for the First GARP Global Experiment*. GARP Publ. Ser., No. 14, 262 pp.

Zheng, Q., and K.-N. Liou, 1986: Dynamic and thermodynamic influences of the Tibetan Plateau on the atmosphere in a general circulation model. *J. Atmos. Sci.*, **43**, 1340-1354.